5-2019

Transcriptional influence of retinoic acid and its effects on angiogenesis of murine salivary glands.

Isaac Feinn
University of Louisville

Follow this and additional works at: https://ir.library.louisville.edu/honors

Part of the Dentistry Commons, Developmental Biology Commons, and the Genetic Processes Commons

TRANSCRIPTIONAL INFLUENCE OF RETINOIC ACID AND ITS EFFECT ON ANGIOGENESIS OF MURINE SALIVARY GLANDS

By

Isaac Feinn

Submitted
in Partial Fulfillment of the Requirements for Graduation *summa cum laude*
and for Graduation with Honors from the Department of Biology

University of Louisville
Louisville, Kentucky

May, 2019

Vasculogenesis and Gene Characterization in *Rdh10* Knockdown Mice

By

Isaac Feinn

A Thesis Approved on

March 25th, 2019

By the following Thesis Committee

_____
Dr. David Schultz

_____
Dr. Lisa Sandell

_____
Dr. Mark Running

Abstract

Salivary gland hypofunction is a major disorder of salivary glands, and can arise either from diseases such as xerostomia, or from defective epithelial morphogenesis during embryogenesis. Hundreds of thousands of individuals suffer from dry mouth, and there is currently no restorative therapy for these patients. Investigation of salivary gland developmental biology will inform regenerative therapies. Currently it is known that retinoic acid (RA), the biologically active form of Vitamin A, is required for proper development of the salivary gland, but little is known about its cellular mechanism regulating organogenesis. This study sought to analyze salivary gland development in *Rdh10* knock down mice to determine if vascular development is impaired, to quantify expression of candidate genes known to be both targets of RA signaling and be involved in angiogenesis, and then identify novel angiogenic genes. We show that retinoic acid signaling alters expression of genes involved in angiogenesis in *Rdh10* knockdowns. Using RNAscope, immunocytochemistry, and qPCR, we characterize the expression and location of *Ctgf* and its protein product, a gene known to aid blood vessel formation. This is the first study to characterize a vascular phenotype associated with *Rdh10* mutants, and identify angiogenic gene targets of RA signaling in *Rdh10* mutants.

LIST OF FIGURES

TABLE OF CONTENTS

INTRODUCTION

Salivary glands are essential for oral health, and loss of their function results in xerostomia, dysphagia, malnutrition, oral mucositis, oral discomfort, and increased oral infections (Cady, 2007; Hancock, Epstein, & Sadler, 2003; Nguyen et al., 2007). Head and neck cancer treatment causes significant damage to salivary gland functioning, and each year 50,000 new cases of this cancer are diagnosed in the United States, while globally it ranks as the 5th most common malignancy (Seiwert, Salama, & Vokes, 2007). Certain autoimmune diseases also impair saliva secretion, such as Sjogren's syndrome, which is estimated to impact greater than 0.4% of the global population (Patel & Shahane, 2014). Therefore, there is a need to develop therapies, which requires knowledge about salivary gland biology. Currently, researchers attempting to design therapies are investigating two possible approaches for remedying loss of salivary gland tissue and functioning: regenerating existing viable tissue, and initiating salivary gland growth from non-salivary gland tissue (Lombaert, Isabelle et al., 2016). Studying how a submandibular salivary gland (SMG) grows and branches within a mouse embryo informs methods to design therapies seeking to achieve salivary gland repair by either of these approaches.

Embryonic murine SMG development initiates on embryonic day 11.5 (E11.5) when thickening occurs of buccal epithelium on either side of the developing tongue (Tucker, 2007). By E12.5, this epithelium has extended into a surrounding mesenchyme to form a preliminary bud before undergoing branching morphogenesis, canalization, and cell differentiation. Angiogenesis occurs concurrently (Fig. 1), and the developing vasculature directs epithelial patterning and differentiation (Kwon, Nelson, DeSantis, Morrissey, &

Larsen, 2017). Beyond the vasculature's standard function of providing nutrients to the organ, for developing salivary glands it has been shown to define the branching structure and organization during morphogenesis. This vasculature can be visualized in the developing embryo by immunostaining for endothelial cells, which are positive for the marker Cluster Differentiation 31 (CD31).
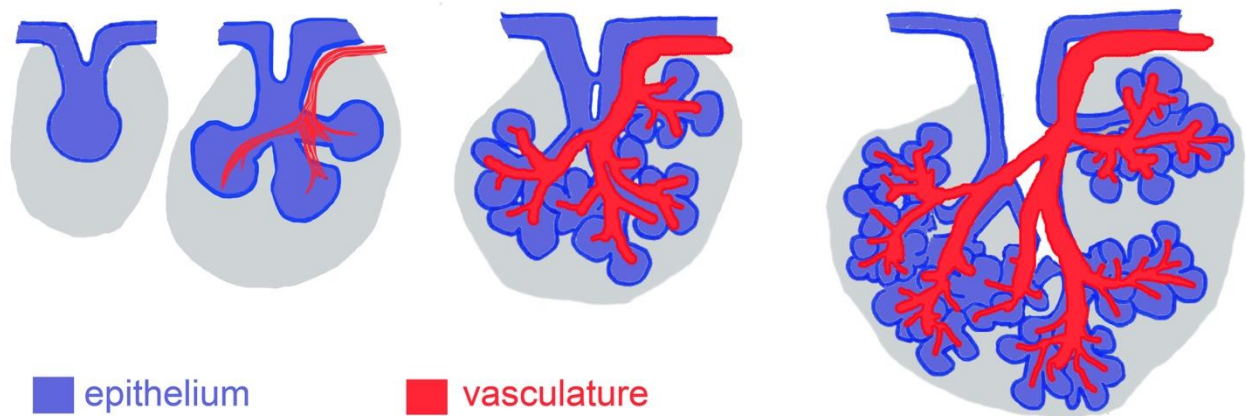
Figure 1. Diagram highlighting how the vasculature develops concurrently with epithelium and participates in defining an embryonic mouse salivary gland's morphology.

Salivary gland patterning and morphogenesis are regulated by retinoic acid (RA) (Wright et al., 2015), which is the biologically active form of retinol, commonly known as Vitamin A (Niederreither & Dolle, 2008). Retinol is typically absorbed through an organism's diet, and is then metabolized to RA in two reactions, the first of which is mediated by retinol dehydrogenase 10 (RDH10) (Sandell, Lynn, Inman, McDowell, & Trainor, 2012; Sandell et al., 2007). Once formed, RA acts as a ligand by binding to specific nuclear transcription factors called retinoic acid receptors located both in the cytosol and at target DNA elements; this complex dimerizes with the Retinoid X

Receptor (RXR) and activates transcription of developmental genes (Metzler & Sandell, 2016) (Fig. 2).
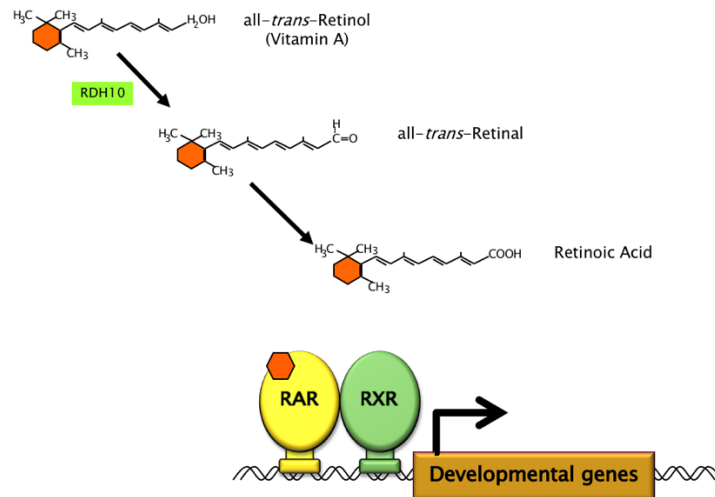
Figure 2. Diagram detailing the metabolic transformation of Vitamin A (all-trans-Retinol) to Retinoic Acid and this molecule's transcriptional activity.

Rdh10 mutant mice, which have deficient RA production, have defective SMG morphogenesis (Wright et al, 2015). The canonical RA signaling transpires in several associated embryonic salivary gland tissues, including epithelium, accompanying parasympathetic ganglion neurons, and non-neuronal mesenchyme (Abashev, Metzler, Wright, & Sandell, 2017), but it is not currently known if it occurs in vascular tissue. While loss of RA signaling leads to defective salivary gland branching, the mechanism for this malformation is not fully understood. However, given the known role for RA in regulating gene transcription, it is likely that the *Rdh10*^{-/-} mutant salivary gland phenotype (Fig. 3) arises from altered gene expression.
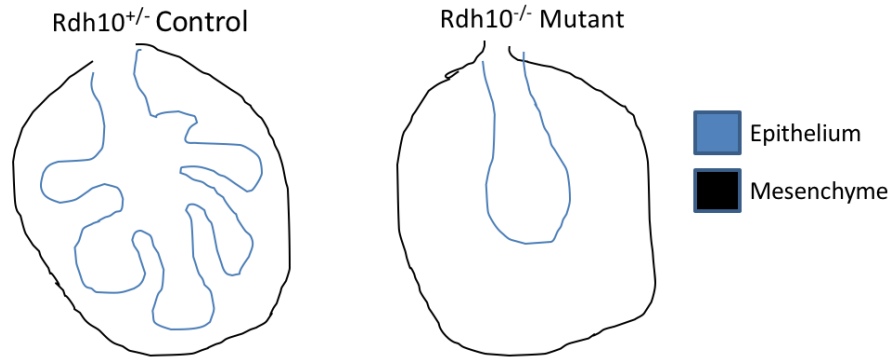
Figure 3. Drawing representing the epithelial-branching defects shown in a murine mutant salivary gland whose gene encoding *Rdh10* has been conditionally knocked out.

Unpublished data from the Sandell Lab show multiple genes are downregulated in a cultured salivary gland whose RA signaling was blocked by BMS493 (Griebel & Sandell, unpublished), a pharmacological pan-RAR inhibitor (Klein et al., 1996). Many of the these gene targets of RA signaling are involved in angiogenesis. One such gene, *Ctgf,* encodes Connective Tissue Growth Factor, a protein that stimulates the production of endothelial basement membrane components such as collagen IV, allowing for adhesion of pericytes to associated endothelial cells (Ponticos, 2013). Due to these factors, *Ctgf* has been shown to be essential for vascular development by regulating endothelial-perictye interactions (Hall-Glenn, 2012). Additionally, *Ctgf* is necessary for lung capillary formation and branching morphogenesis (Wu S, Platteau A, Chen S, McNamara G, Whitsett J, Bancalari E, 2010). For thess reasons, *Ctgf* was chosen as the principal candidate gene for exploration into the potential relationship between RA and angiogensis.

Preliminary experiments for the current study established there is a vascular phenotype associated with *Rdh10* mutants. Seeking to establish a mechanistic connection between lack of RA signaling and a predicted vascular phenotype, this study then

attempts to characterize the principal candidate gene *Ctgf* by quantifying its expression in *Rdh10* knockouts *in vivo* and localizing its mRNA transcript and gene product within a developing salivary gland. Furthermore, the additional candidate genes identified in the cultured inhibition of RA signaling will be analyzed for changes in gene expression within an *Rdh10* mutant. Lastly, this study examines expression rates in *Rdh10* mutants of all genes known to be involved in angiogenesis of a developing salivary gland in order to identify genes requiring transcriptional activation by RA signaling to facilitate angiogenesis. This study also validated the altered retinoid homeostasis in salivary glands of *Rdh10* mutant embryos by examining expression levels in *Rdh10* mutants of genes involved in the metabolism of Vitamin A.

This study has the potential to expand the knowledge regarding the mechanism by which Vitamin A regulates salivary gland development. Because developing vasculature has been shown to direct the morphology of budding epithelium in a salivary gland, it is possible that reduced expression of genes critical to angiogenesis due to loss of RA signaling could give rise to the defective phenotype observed in Vitamin A deficient mice. Knowledge of proteins encoded by genes such as *Ctgf* with altered expression in *Rdh10* knockdowns could provide a mechanistic link between Vitamin A and impaired endothelial branching morphogenesis. Additionally, gene expression levels reported by *in vivo* qPCR analysis of angiogenic candidate genes in *Rdh10* knockouts in this study can be compared with those conducted *in vitro* to further understand how these genes are regulated. Lastly, the results from qPCR and DNA array analysis can inform future experiments regarding what genes to investigate to further explore Vitamin A's role in murine SMG organogenesis.

HYPOTHESIS

Rdh10 conditional mutant submandibular glands will have disrupted vasculogenesis compared to controls and this will correlate with the misexpression of genes, such as *Ctgf*, known to play a role in blood vessel development.

METHODS

Animals. The generation of the mutant ($Rdh10^{delta}$) and conditional ($Rdh10^{flox}$) alleles has been described previously (Sandell et al., 2012). In order to knock out the conditional $Rdh10$ allele by recombination, this study also included mice carrying the cre-*ERT2* allele (Ventura et. al., 2007). To generate litters containing both $Rdh10$ conditional mutant and $Rdh10$ heterozygote control embryos, $Rdh10^{delta/+}$ mice were set up in a timed mating with $Rdh10^{flox/flox};ERT2^{*2}$ mice. Day of vaginal plug was considered E0.5. We have previously shown that these litters contain ~50:50 $Rdh10^{delta/flox};ERT2$ (conditional mutant) and $Rdh10^{flox/+};ERT2$ (heterozygote control) embryos (Metzler et. al., 2018). To knock out the conditional $Rdh10$ allele in embryos, pregnant dams were administered 5mg Tamoxifen + 2mg Progesterone in 250µl corn oil by oral gavage on day E8.5 as described in Metzler et al. (2018). All mice were maintained at the University of Louisville, and all experiments using mice were preformed according to a protocol approved by the Institutional Animal Care and Use Committee at the University of Louisville.

Acquisition of cDNA and Quantitative Polymerase Chain Reaction. SMGs were dissected from embryonic mice at E13.5. RNA from their SMG was then extracted and isolated using RNeasy Micro Kit (Qiagen). This RNA was then converted to cDNA via a reverse transcriptase from Super Script III (Invitrogen). The resulting cDNA underwent a polymerase chain reaction to quantify the gene expression of vasculature genes such as CD31 using Angiogenesis RT^2 Profiler PCR Array (Qiagen).

RNAscope. In situ hybridization assay from Advanced Cell Diagnostics was used to visualize the location of the target RNA within developing SMGs. SMG samples were harvested at E13.5, sectioned, and then paraffinized. After the slides had baked for an hour at 60°C, they were deparaffinized to allow for target retrieval using a Tissue Tek jar containing Target Retrieval solution in a steamer. The slides were then left in a humidifying box overnight. After a series of prepping reagents, the probe Mm-CTGF-C2 was added to each slide. Next, AMP1, AMP2, and AMP3 were added between 30 minute incubations in the HybEZ oven. The fluorophore solutions were then added: HRP-C1, Opal 520, and HRP-blocker, followed by DAPI. The slides were sealed using Prolong Gold and coverslip.

Immunocytochemistry. SMG explants underwent whole mount immunostaining as carried out by the Sandell lab in 2017 using identical protocol (Abashev et al., 2017). The primary antibody used was the anti-CD31 antibody ab28364 (Abcam), while the secondary will be Alexa Fluor 546 Goat Anti-Rabbit IgG (H+L) A-11010 (Invitrogen). Images were viewed using a Zeiss AX10 confocal microscope.

Wholemount staining of vasculature. Whole SMGs were dissected from E13.5 embryos and fixed in 10% NBF. Immunostaining wholemount was performed as previously described (Abashev et. al., 2017). Primary antibodies used were anti-CD31 (abcam ab28364, 1:50) and anti-TUBB3 (BioLegend MMS-435P, 1:1000). Secondary antibodies used were Alexa Fluor 546 (ThermoFisher A-11003, 1:300) and Alexa Fluor 660 (ThermoFisher A-21054, 1:300).

Wholemount imaging. Imaging was performed on a Leica SP8 confocal microscope with solid state lasers 405, 488, 552, and 638nm. Z-stacks were rendered into image projections using the software Imaris.

RESULTS

Vascular Phenotype Associated with *Rdh10* Mutants

Embryonic salivary glands of *Rdh10* mutants produce endothelial tissue, but cannot form continuous blood vessels

To determine whether RA signaling is required for angiogenesis in a murine salivary gland, cluster of differentiation 31 (CD31; PECAM1 – Mouse Genome Informatics)[+] vasculature was examined on E13.5 *Rdh10* knockdown salivary glands. SMG explants dissected and paraffinized on E13.5 underwent whole mount immunostaining using the anti-CD31 antibody ab28364 (Abcam). The following six images are each from separate animals. On left, the animals are capable of metabolizing Vitamin A, while those animals shown on right cannot. This accounts for the difference in epithelial branching shown in all samples between the controls and mutants. Defective branching is a known phenotype in *Rdh10*^{-/-} conditional mutants. These images show that endothelial cells (shown in red fluorescence) are present in mutants; however, observing blood vessel morphology is difficult in 2D sections.

Cross-sectional comparison of vasculature in control and *Rdh10* mutant mouse SMG

Rdh10$^{+/-}$ Rdh10$^{-/-}$
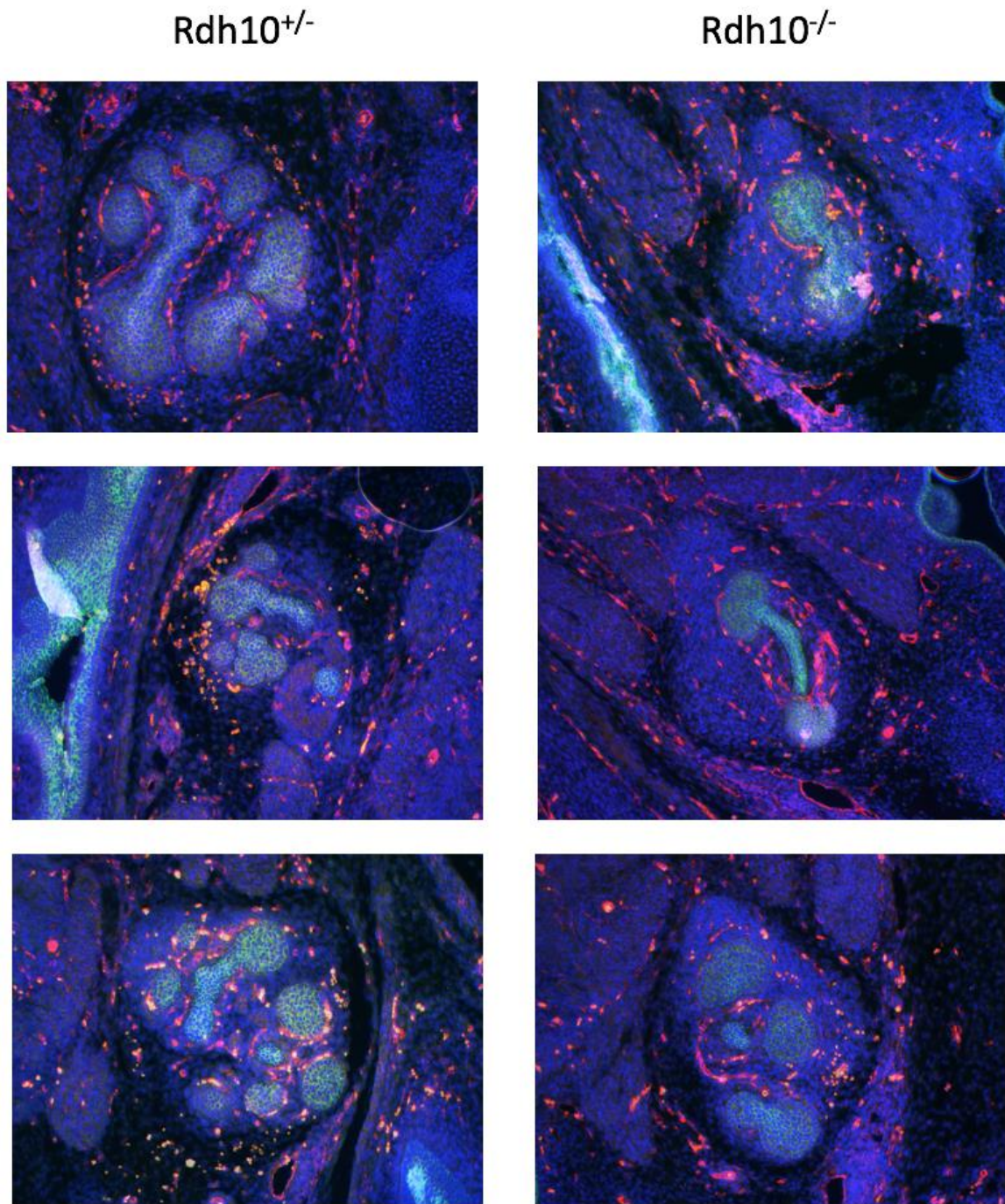
Figure 4. **Vasculature is present in developing salivary gland of *Rdh10* mutants.**

Salivary glands were dissected from embryos and paraffinized on E13.5. Cross sections

are taken in the frontal plane. Heterozygous controls (*Rdh10$^{+/-}$*) are shown on left while

conditional knockdowns (Rdh10$^{-/-}$) are shown right. All cells appearing blue are stained

with DAPI, a molecule that binds to the minor groove of double stranded DNA. The neon

green pigmentation shows cells stained with anti-E-cadherin, an antibody that binds the

epithelial tissue within the salivary gland. The red and yellow pigmentation shows cells

stained with Cluster of Differentiation 31 (CD31), otherwise known as Platelet

Endothelial Cell Adhesion Molecule (PECAM), which binds endothelial cells and serves

as a marker for angiogenesis. Autofluorescence naturally emitted from biological

structures was imaged in dark green. Images were viewed through a Zeiss AX10

fluorescent microscope, and represent merges of separate images taken at different

wavelengths to capture the fluorescence of each secondary antibody. The merged image

changes the autofluorescence to a desaturated gray color which aids in distinguishing true

signals from naturally occurring ones.

Because the previous image (Fig. 4) analyzed the glands only in cross-section, the

3D structure of the vasculature of an *Rdh10* mutant salivary gland remained unknown. In

order to visualize the multi-dimensional organization of SMG endothelial tissue,

wholemount staining with CD31 was conducted on E13.5 SMG explants. Wholemount

immunostaining was performed as previously described (Abashev et. al., 2017). Primary

antibodies used were anti-CD31 (abcam ab28364, 1:50) and anti-TUBB3 (BioLegend

MMS-435P, 1:1000). The following images show that vasculature is underdeveloped in

SMG explants of *Rdh10* knockdown mice. In mutant glands, endothelial cells are still

present, but are unable to form elongated blood vessels.

Wholemount comparison of vasculature in control and mutant mouse SMG
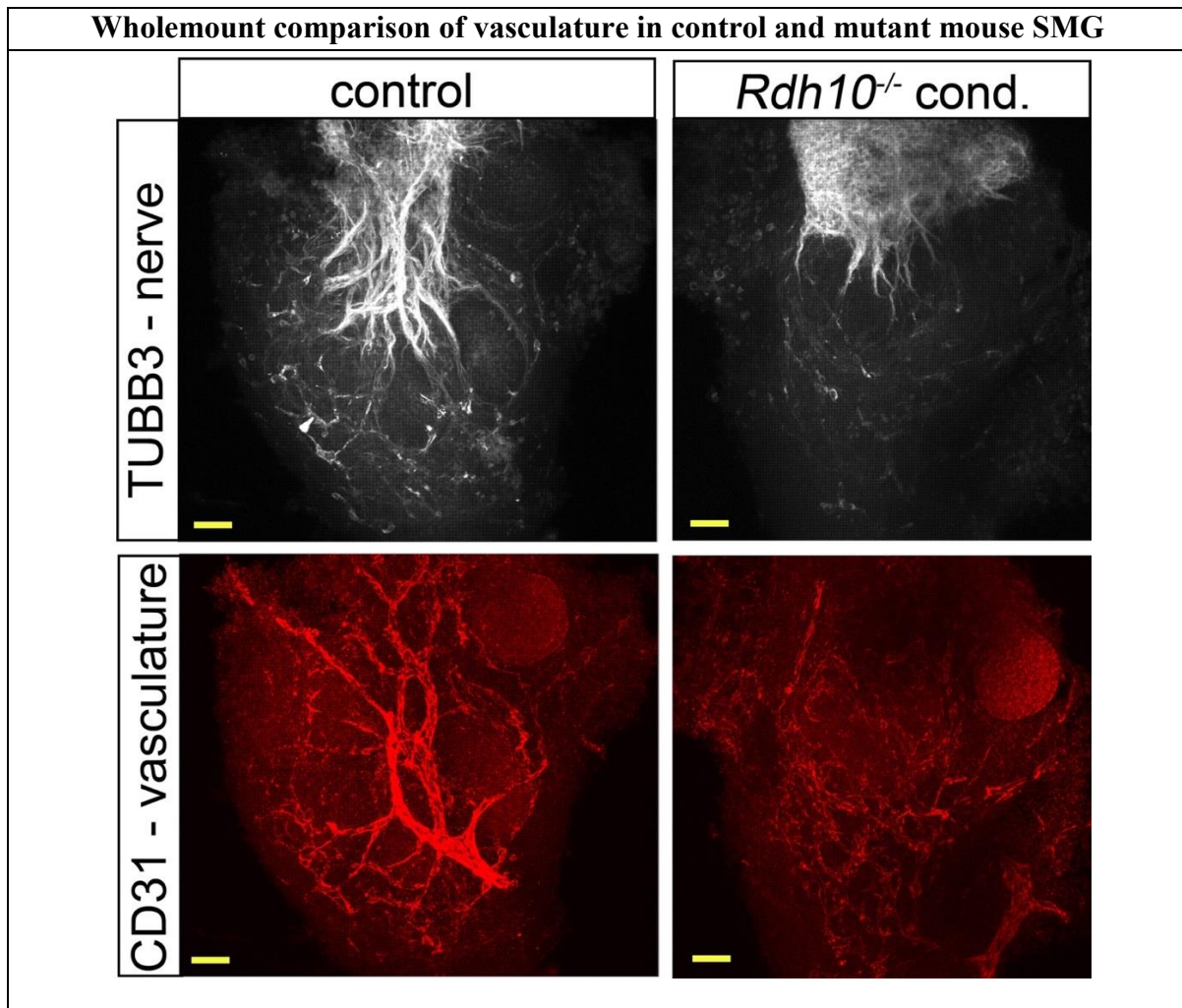
Figure 5. *Rdh10* **mutants cannot form continuous blood vessels.** SMG at E13.5 of heterozygous controls (*Rdh10*^{+/-}) are shown on left while conditional knockdowns (*Rdh10*^{-/-}) are shown on right. Whole SMGs were dissected from E13.5 embryos and fixed in 10% NBF. Immunostaining wholemount was performed as previously described (Abashev et. al., 2017). Imaging was performed on a Leica SP8 confocal microscope with solid state lasers 405, 488, 552, and 638nm. The primary antibody anti-TUBB3 binds nerve tissue, while anti-CD31 binds endothelial tissue. This experiment was conducted by Melissa Metzler, an associate researcher in Lisa Sandell's lab at the University of Louisville School of Dentistry. Mutant explants show no presence of elongated vasculature.

Investigation of Candidate Angiogenic Genes

Principal candidate gene *Ctgf* is expressed in spatially restricted domains of salivary glands but is unchanged in *Rdh10* mutants

The vascular phenotype discovered to be associated with *Rdh10* knockdowns indicated that lack of RA signaling may result in dysregulation of genes critical to angiogenesis. *Ctgf* was chosen as this study's principal candidate gene for characterization within a developing salivary gland because it is known to be a direct target of RA signaling (Delacroix et al, 2009), downregulated in RA signal inhibited salivary glands (Griebel & Sandell, unpublished), and necessary for lung capillary formation and branching morphogenesis (Wu S, Platteau A, Chen S, McNamara G, Whitsett J, Bancalari E, 2010).

Previous transcriptional analyses has demonstrated that *Ctgf* is expressed in salivary glands (NIDCR, Salivary Gland Atlas), but the whole gland spatial distribution has not been studied. In order to define the whole gland tissue localization of *Ctgf* RNA expression in normal salivary glands, RNAscope was performed *in situ* hybridization on paraffinized frontal sections of E13.5 wild type salivary glands. Red punctate dots show single *Ctgf* mRNA molecules bound to double Z RNAscope® Probes, a fluorescing technique that utilizes a ~20 nucleotide target-specific probe hybridized to target RNA molecules and is amplified by multiple label probes. *Ctgf* transcripts were observed to localize in epithelial tissue, while mesenchymal tissue appeared to have little or no *Ctgf* RNA (Fig. 6). Furthermore, transcripts are most concentrated near the base of endbuds, but additional samples would need to be gathered to confirm if this is representative of *Ctgf* expression in salivary glands.

Location of *Ctgf* mRNA in mouse SMG cross-section
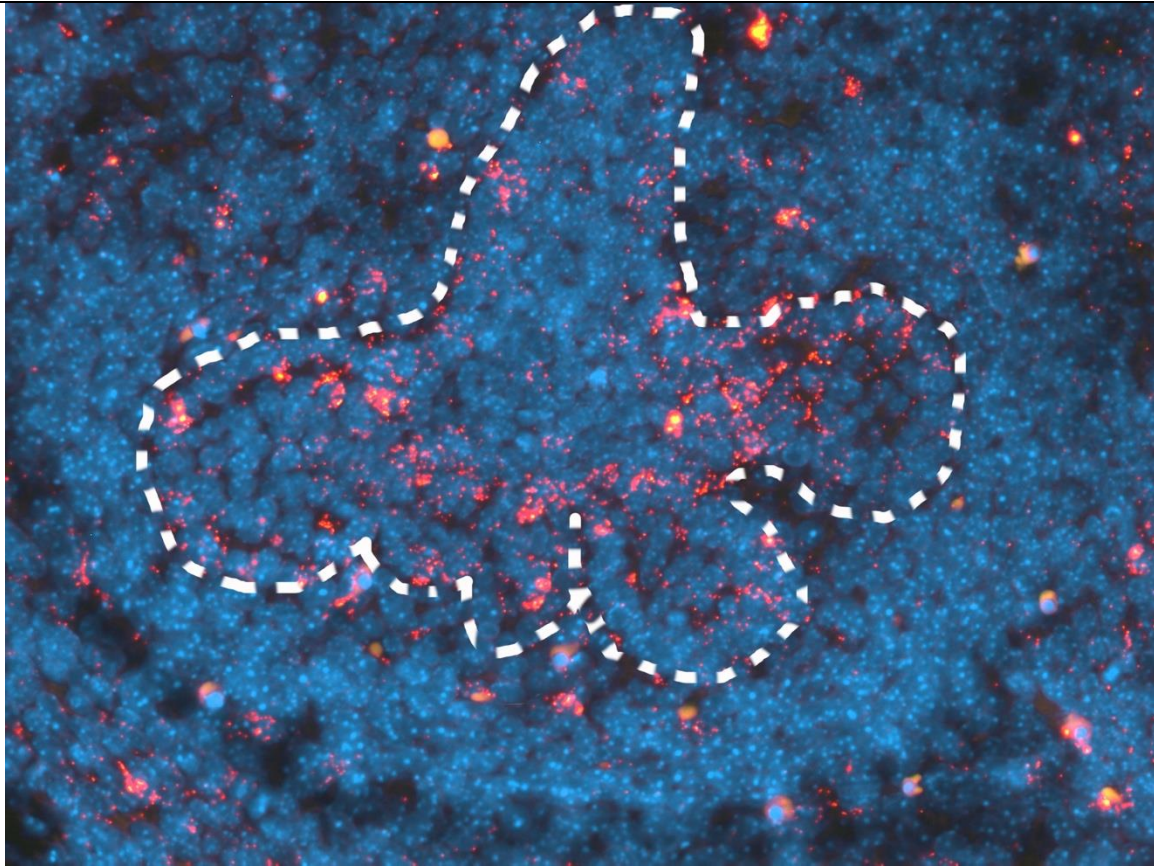
Figure 6. *Ctgf* **mRNA localizes to epithelial tissue of SMG at E13.5.**

Frontal section of E13.5 SMG from wild type mouse embryo with *Ctgf* RNA labeled by RNAscope *in situ* hybridization. Red signal indicates *Ctgf* RNA. Blue is all nuclei labeled with DAPI. Epithelium is outlined by white line. *Ctgf* RNA is localized within epithelium, but is scarcely detected in the surrounding mesenchyme.

Although the previous experiment defines the expression pattern of *Ctgf* RNA, the localization of the *Ctgf* protein within a developing salivary gland was previously unknown. To visualize the localization of CTGF protein in a developing salivary gland, immunocytochemistry was performed on wild type salivary gland sections using anti-CTGF antibody. Dissection of normal salivary glands occurred on E13.5, and samples

were paraffinized, sectional frontally, and stained using anti-CD31 antibody ab28364 (Abcam). CTGF appears to localize at the base of ducts in a pattern similar to known neuron innervation. No significant CTGF staining was observed in the mesenchyme or epithelium.

Location of CTGF protein in mouse SMG cross-section

Figure 7. CTGF protein in SMG cross-section at E13.5 localizes near ducts in pattern reminiscent of neuronal structures. Frontal section of E13.5 wild type embryo SMG stained with anti-CTGF antibody and imaged through a Zeiss AX10 fluorescent microscope. High
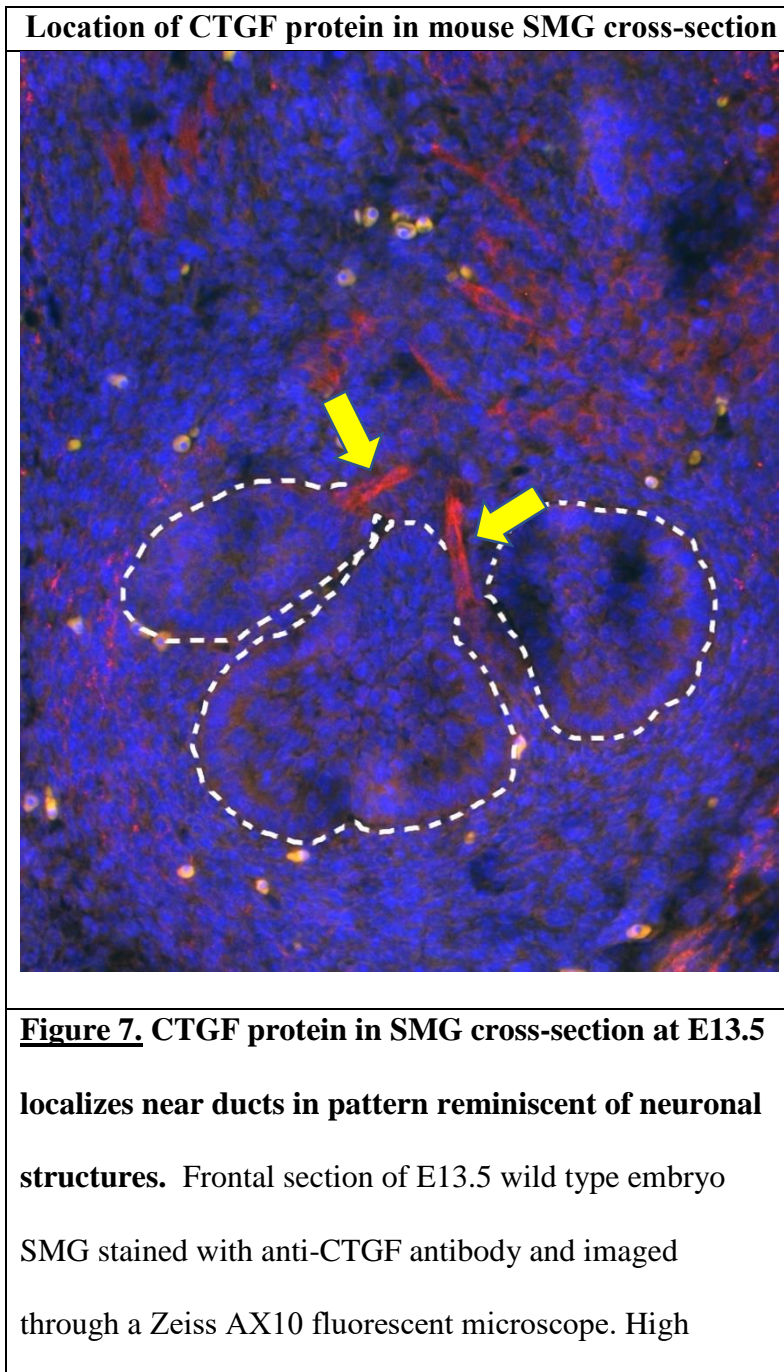
concentration of CTGF protein (denoted by yellow arrows) is detected at base of endbuds in region known to be occupied by parasympathetic nerve. Red fluorescence indicates presence of CTGF, while blue indicates nuclei of all cells stained with DAPI. Epithelium is outlined by white line. In this section only endbuds are visible and ducts are not within the plane of the section.

Previous experiments identifying genes of RA signaling were conducted using the pharmacological inhibitor BMS (Griebel & Sandell, unpublished), but it was not known if gene expression would be similarly altered in salivary glands of *Rdh10* mutant embryos *in vivo*. To test this, a qPCR array examining genes associated with vasculogenesis analyzed gene expression in *Rdh10* mutants relative to controls. RNA was extracted from SMG of *Rdh10* mutant embryos on E13.5 and converted to cDNA for qPCR analysis. The array analyzed cDNA samples from three heterozygous controls (*Rdh10*$^{+/-}$) and three conditional knockouts (*Rdh10*$^{-/-}$), and the average delta Ct values from each group are presented in the figure below. Although *Ctgf* has reduced expression in salivary glands cultured with BMS, this *in vivo* analysis shows that expression of *Ctgf* is not significantly altered in *Rdh10* mutant salivary glands (Fig 8).

Relative expression of *Ctgf* in *Rdh10* mutants					
	Ct. H1-3 Avg.	Ct. M1-3 Avg.	p.value	t.statistic	log2 foldchange
Ctgf	9.01	9.26	0.498	-0.74356	-0.02541
Figure 8. *Ctgf* **expression is not changed in** *Rdh10* **mutant.**					

Gene expression rates were measured using a Qiagen RT PAMM-024ZA-6 "Mouse Angiogenesis" Profiler Array. The plate examined 77 genes known to be involved in murine angiogenesis. Six cDNA samples were used in total: three heterozygous controls ($Rdh10^{+/-}$) and three conditional knockouts ($Rdh10^{-/-}$). Six RT Profiler Array plates were used: one for each cDNA sample. The average Ct values for the heterozygous controls are shown in the second column, while the average for the mutants is shown in the third. The P-value associated with the change in expression between the mutants and controls was 0.498. The housekeeping gene used for this experiment was *Gapdh*.

Additional angiogenic candidate genes are not altered in *Rdh10* mutants

Because the principal candidate gene *Ctgf* had no change in expression in *Rdh10* mutants, the additional candidate genes identified in previous studies (Griebel & Sandell, unpublished) were similarly analyzed for expression changes in *Rdh10* mutants. These genes, which are known to facilitate angiogenesis, were grouped into two categories: those involved in extracellular matrix processes, and those involved in the production of developmental growth factors. For each gene studied, the cDNA from SMG of three heterozygous controls ($Rdh10^{+/-}$) and three conditional knockouts ($Rdh10^{-/-}$) were analyzed. qPCR was used to analyze the relative expression of these genes in an *Rdh10* mutant salivary gland. RNA was extracted from SMG of *Rdh10* mutant embryos on E13.5 and converted to cDNA for qPCR analysis. Primers for these genes were designed

for use in qPCR, and in order to assess primer efficiencies, qPCR was performed on five-fold serial dilutions of DNA. Primers that regressed within 90-110% of the line of best fit were selected for further use in quantitative assays. These analyses can be found in Analysis of Primer Efficiencies in the Supplemental Figures of this study. All qPCR analyses used primers with validated efficiencies. The expression of all candidate genes associated with extracellular matrix processes and developmental growth factors was unchanged in *Rdh10* mutants (Fig. 9, Fig. 10). These data demonstrate that the vascular phenotype observed in Fig. 5 is not due to altered regulation of these genes.

Gene expression in *Rdh10* knockdowns of extracellular matrix process genes
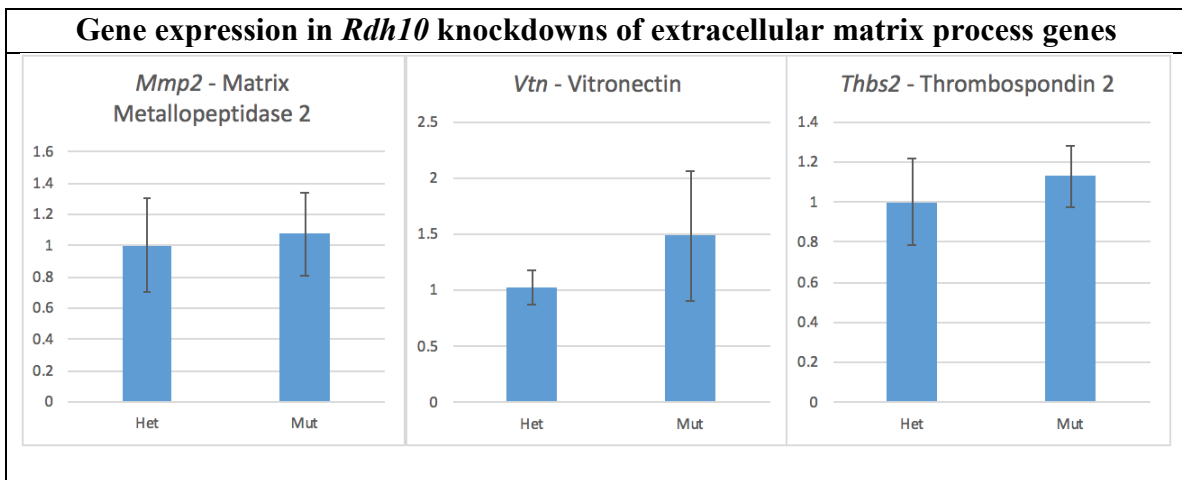
Figure 9. **Expression rates of extracellular matrix genes *Mmp2, Vtn,* and *Thbs2* are unchanged in SMG of *Rdh10* mutants.** Gene expression was measured using an Applied Biosystems 7500 Real-Time qPCR System. Relative expression graphs are constructed comparing the ΔΔCt values examined in murine cDNA of heterozygous controls (*Rdh10*$^{+/}$) to conditional mutants (*Rdh10*$^{-/-}$). These results are normalized to *Gapdh,* and represent the average between three controls and three mutants. Expression rates of these genes are not changed in the mutants.

Gene Expression in *Rdh10* knockdowns of developmental growth factor genes

Figure 10. Expression rates of *Bmp4, Igf1, Fgf8, Bmp2, Fgf7,* and *Fgfr2b* are unchanged in *Rdh10* mutants. Gene expression was measured using an Applied Biosystems 7500 Real-Time qPCR System. Relative expression graphs are constructed comparing the ΔΔCt values examined in murine cDNA of heterozygous controls (*Rdh10*$^{+/-}$) to conditional mutants (*Rdh10*$^{-/-}$). These results are normalized to *Gapdh,* and represent the average between three controls and three mutants. Expression rates of these genes are not changed in the mutants.
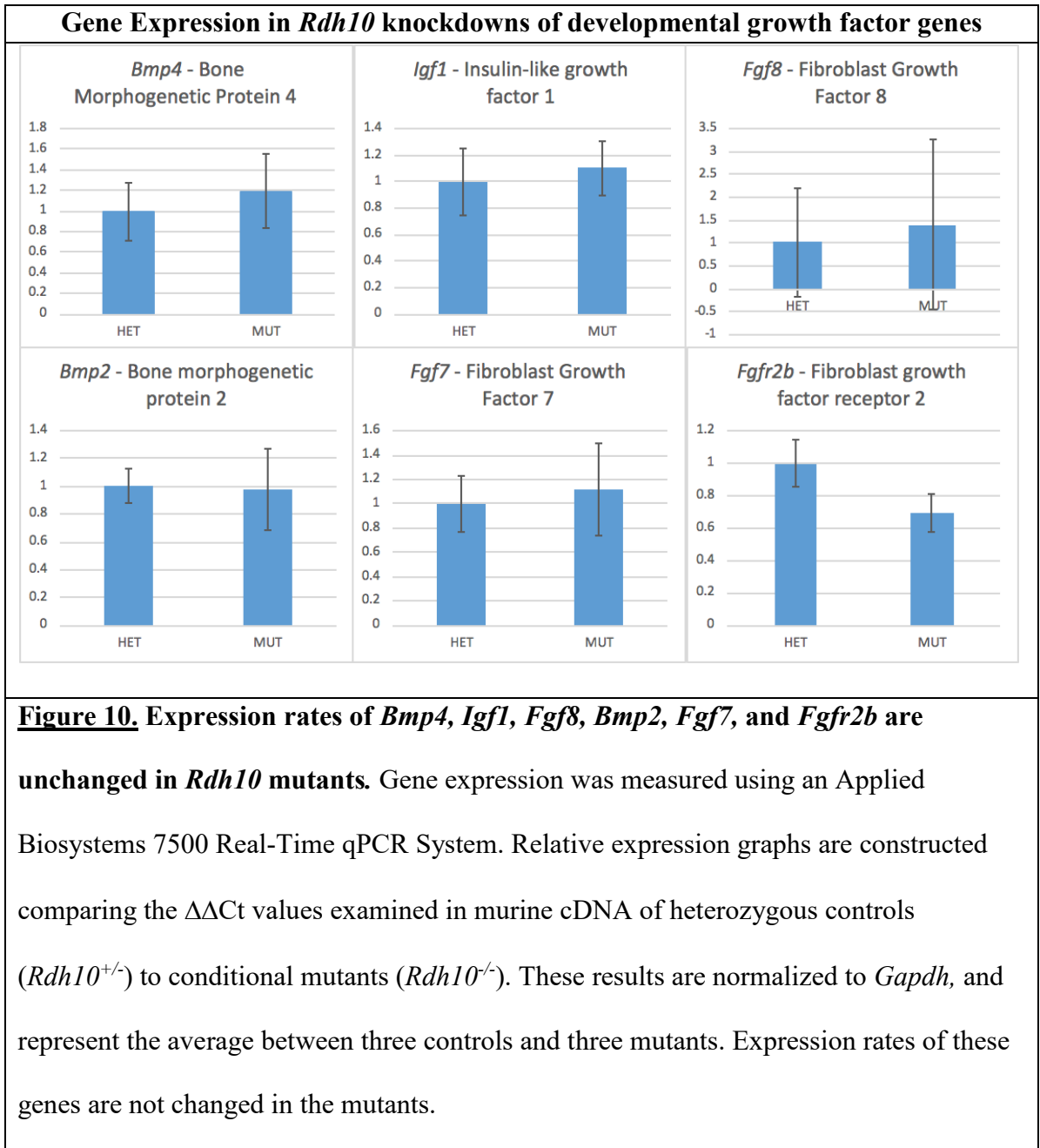
Five angiogenic genes discovered to be altered in *Rdh10* mutants

Because the characterization of this study's candidate genes indicated that none of them experienced altered expression in *Rdh10* mutants, we sought next to identify novel genes that were perturbed in *Rdh10* mutant SMG to gain insight as to how RA signaling gives rise to the vascular phenotype discovered in *Rdh10* mutants. In order to examine the expression of all genes known to be associated with angiogenesis in a salivary gland, a qPCR array was used to analyze cDNA from *Rdh10* mutant SMG. The following data were gathered using a Qiagen RT PAMM-024ZA-6 "Mouse Angiogenesis" Profiler Array. The plate included 77 genes known to be involved in murine angiogenesis. Six cDNA samples converted from RNA that was harvested from E13.5 SMGs were used in total: three heterozygous controls ($Rdh10^{+/-}$) and three conditional knockouts ($Rdh10^{-/-}$). Six RT Profiler Array plates were used: one for each cDNA sample. Of the 77 genes examined, five showed statistically significant changes in transcript abundance in mutants compared to controls. These genes are the following: *Angpt2, Jag1, Mapk14, Ptgs1,* and *S1pr1* (Fig. 11, 12). All genes except *S1pr1* were downregulated in *Rdh10* mutants, while *S1pr1* was upregulated.

Delta CT values						
	Ct.B1275.H1	Ct.B1275.H2	Ct.B1299.H1	Ct.B1275.M1	Ct.B1275.M2	Ct.B1299.M1	p.value
S1pr1	5.9914	5.937	5.9711	5.474	5.454	5.3338	0.000303
Angpt2	8.5574	8.7536	8.3373	9.7673	9.5177	9.5468	0.001796
Jag1	5.6459	5.4903	5.3719	5.9745	5.7919	5.9146	0.0151
Ptgs1	9.3267	8.9818	8.6138	9.608	9.8959	9.7548	0.024707
Mapk14	5.3609	5.5119	5.4247	5.598	5.544	5.6919	0.043798

Figure 11. **Genes *s1pr1, Angpt2, Jag1, Ptgs1,* and *Mapk14* are altered in *Rdh10* mutants.** Delta Ct values of three heterozygous controls and three *Rdh10* mutants are shown. This table is arranged in increasing P value. These data were found using the Qiagen RT PAMM-024ZA-6 "Mouse Angiogenesis" Profiler Array. Dissections of SMG

from embryos occurred on E13.5, after which RNA extraction and conversion to cDNA

took place. Five genes, *s1pr1, Angpt2, Jag1, Ptgs1,* and *Mapk14,* are altered in *Rdh10*

mutants.

Relative expression of altered angiogenic genes in *Rdh10* mutants
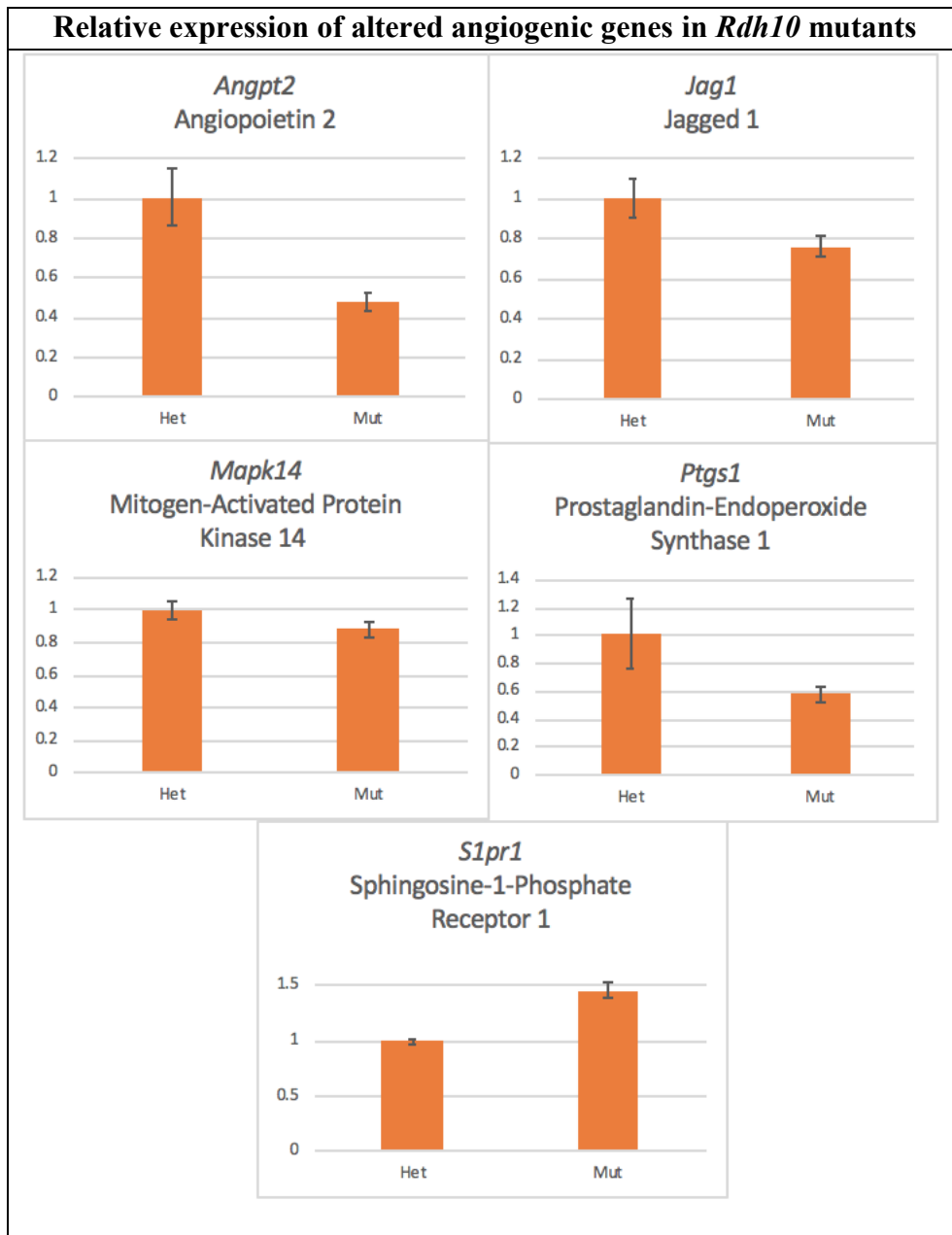
Figure 12. *Angpt2, Jag1, Mapk14, and Ptgs1* **are downregulated while**

S1pr1 **is upregulated in *Rdh10* mutants.** Relative expression (measured

by ∆∆CT) of angiogenic genes which showed a significant change in mutants compared to control. These data were found using the Qiagen RT PAMM-024ZA-6 "Mouse Angiogenesis" Profiler Array. Dissections of embryos occurred on E13.5, after which RNA extraction and conversion to cDNA took place. Four of these genes are down-regulated and one is up-regulated. Samples with significant p-values are shown in orange. These data show RA signaling is required for the proper expression of these five genes that are associated with vascular development.

Three genes involved in the metabolism of Vitamin A found to have altered expression in *Rdh10* mutants

These genes were studied as part of a supplemental project carried out in the Sandell Lab, and are not associated with angiogenesis in a developing salivary gland. In order to assess how the salivary gland responds to a lack of RA and its signaling, these genes were analyzed for changes in expression rates. Dissection of embryos occurred on E13.5, and RNA extraction and conversion to cDNA was completed afterwards. The qPCR analyses of these genes included cDNA samples from three heterozygous controls ($Rdh10^{+/-}$) and three conditional knockouts ($Rdh10^{-/-}$). Three genes were found to have altered expression in *Rdh10* mutants: *Aldh1a1, Aldh1a2,* and *Cyp26a1* (Fig. 13). The altered expression of these genes validates perturbation of RA homeostasis in SMG of *Rdh10* mutant embryos.

Relative expression of Vitamin A metabolic genes in *Rdh10* mutants

Figure 13. **Expression rates of *Aldh1a1, Aldh1a2,* and *Cyp26a1* are altered in *Rdh10* mutants, while those of *Cyp26b1, Dhrs3, RARb,* and Stra6 are unchanged.** Gene expression was measured using an Applied Biosystems 7500 Real-Time qPCR System. Relative expression graphs are constructed comparing the ΔΔCt values examined in murine cDNA of heterozygous controls (*Rdh10*$^{+/-}$) to conditional mutants (*Rdh10*$^{-/-}$). These results are normalized to *Gapdh,* and represent the average between three controls and three mutants. Samples with significant p-values are shown in orange. A two-sample t-Test assuming equal variances showed a one-tailed P value for *Aldh1a1* of 0.033, *Aldh1a2* of 0.042, and *Cyp26a1* of 0.036. *Aldh1a1* and *Cyp26a1* are downregulated while *Aldh1a2* is upregulated in *Rdh10* mutants.

DISCUSSION

This study was the first to examine the effect of blood vessel development on embryonic salivary glands of mouse mutants with impaired Vitamin A metabolism. Although *Ctgf* was not found to be a significant gene target of RA signaling *in vivo*, we demonstrate that salivary glands of *Rdh10* knockdowns have altered expression of genes known to aid in angiogenesis (Fig. 11) as well as having underdeveloped blood vessels (Fig. 5) at E13.5. These findings support the hypothesis that Vitamin A in its biologically active form RA regulates proper development of a salivary gland's vasculature through transcriptional activation.

The hypothesis was based primarily on two previous studies: one that identified genes with altered expression in the absence of RA signaling (Griebel & Sandell, unpublished) and another that found the vasculature's role in developing mouse salivary glands to include instructing epithelial patterning (Kwon, Nelson, DeSantis, Morrissey, & Larsen, 2017). The latter study provided reason to investigate whether RA signaling influences angiogenesis as a possible explanation for the defective epithelial branching observed in *Rdh10* mutants (Wright et al, 2015).

This study hypothesized that immunocytochemistry in mutants who have lost the ability to transcribe *Rdh10*, the enzyme responsible for converting Vitamin A to its metabolically active form, would show defects in vasculature relative to control due to dysregulation of genes critical to angiogenesis. However, cross sectional analysis using CD31 primary antibodies showed no significant change in blood vessel development in mutants compared to controls (Fig. 4). Regardless, this experiment verified that mutants maintain the ability to form endothelial tissue. The imaging appeared to show more

vasculature associated with mesenchyme tissue in the mutants, as the vessels appear to cluster with a higher degree of organization around the epithelial tissue in the controls; however, this observation could result from lack of epithelial development in *Rdh10* knockdowns.

Because cross sectional analysis observes tissue in only two dimensions, an additional experiment examining the whole organ in three dimensions was conducted (Fig. 5). Melissa Metzler conducted the experiment due to time constraints placed on the original researcher. The results indicated an inability of the mutant to form large blood vessels; indeed, the mutant appears only capable of forming small, less organized endothelium. Additionally, nerve development was severely impaired in the mutant as indicated by TUBB3$^+$ cells. These results indicate that protein products of genes targeted by RA signaling are necessary to form continuous blood vessels in a developing salivary gland. Between E11.5 and E12.5, healthy salivary glands develop discontinuous vascular networks within the mesenchyme surrounding the primary epithelial bud (Kwon, Nelson, DeSantis, Morrissey, & Larsen, 2017). At E13.5, elongated vascular networks distinct from TUBB3$^+$ innervation have formed (Kwon, Nelson, DeSantis, Morrissey, & Larsen, 2017). It is likely then that lack of protein products of genes targeted by RA signaling impairs elongated vascular network development between E12.5 and 13.5 either by damaging construction mechanisms or maintenance processes.

To further understand how RA signaling influences vasculogenesis, we then chose to characterize the activity of a candidate gene within a salivary gland that is known both to be regulated by RA signaling and to facilitate SMG angiogenesis. One gene reported to have these qualities *in vitro* is *Ctgf* (Griebel & Sandell, unpublished).

This study used *Ctgf* to serve as a model for RA's influence on vasculogenesis by characterizing its transcript and protein product location in a developing SMG, and quantify its expression *in vivo*.

RNAscope visualized *Ctgf* transcript location (Fig. 6) and found that *Ctgf* mRNA is almost exclusively located in budding salivary gland epithelium, not the mesenchyme. Canonical RA signaling influences epithelium morphogenesis by direct action specifically in the epithelial tissue (Abashev, 2017), which could explain why *Ctgf* transcripts are largely found in epithelial tissue. Cells secrete CTGF into extracellular space to mediate cell adhesion in endothelium (Ponticos, 2013), implying that although *Ctgf* transcripts lie within the epithelium their protein product may not. Additionally, the transcripts appear to localize around the basal lining of the epithelium and form an arch at the base of each endbud's connection to the epithelial duct. These connection points are surrounded by salivary clefts, which are depressions in the basement membrane that subdivide the buds and subsequently define the boundary between the terminal proacinar structure and the emerging secondary ducts. The reason for the increased concentration of *Ctgf* transcript in the clefts is not known; however, CD31 staining in an E13.5 salivary gland shows a high degree of association between the epithelium and vasculature inside clefts (Kwon, Nelson, DeSantis, Morrissey, & Larsen, 2017). Perhaps cleft-enriched *Ctgf* promotes local angiogenesis, giving rise to the numerous blood vessels characteristic of a healthy salivary gland.

Endothelial genes are known to have increased expression at or near these clefts. Quantitative analysis of the epithelial morphology in salivary gland explants treated with an inhibitor for one such endothelial gene, *Vegfr2*, shows reduced branching

morphogenesis (Kwon, Nelson, DeSantis, Morrissey, & Larsen, 2017). This gene encodes the Vascular Endothelial Growth Factor Receptor 2; however, the genes encoding Vascular Endothelial Growth Factors, *Vegfa, Vegfb,* and *Vegfc* did not show any significant altered expression in the qPCR array data (Supplement to Fig. 11). Thus, although RA signaling is required for proper expression of some genes critical to salivary gland angiogenesis (Fig. 11), it does not regulate all genes critical to angiogenesis.

While the *Ctgf* transcripts formed an arched pattern inside the epithelium, the protein product localized in a rod-like shape near the connection between end and primary epithelial buds (Fig 7). CTGF promotes proliferation and differentiation of chondrocytes, and mediates heparin and divalent cation-dependent cell adhesion of fibroblasts, myofibroblasts, and endothelial cells (Ponticos, 2013). Thus, this geometrical concentration of CTGF suggests the protein is localizing to aid in the growth of the epithelial or endothelial structure of the gland. The protein appears to localize to parasympathetic nerve cells, which commonly form near endbud connections to duct during SMG biogenesis and are present as early as E13 (Holmberg, 2014). Its concentration is scarce within the mesenchyme, and most mesenchymal fluorescence can be attributed to autofluorescence.

To conclude the characterization of *Ctgf*, the gene's expression in *Rdh10* knockdown mutants was compared to control expression. As previously mentioned, *in vitro* impairment of RA signaling identified multiple genes with significantly altered expression. However, this RA block was achieved using reverse-agonist BMS493, a non-selective inhibitor of all three retinoic acid receptor (RAR) isoforms. Therefore, RA signaling in SMG cultured with BMS is less than in *Rdh10* conditional knockouts, which

maintain approximately 30% of RA signaling. This technique required the salivary gland to be isolated from the organism and cultured separately, a process that could have impaired unknown cellular mechanisms other than RA signaling and resulted in the observed phenotype. In order to provide supporting data that RA signaling regulates the genes identified in the BMS culture, we used a conditional knockdown for *Rdh10* that allowed the salivary gland to remain intact with the organism until the mRNA extraction. Compared to the use of a chemical inhibitor, the results from our experiment present data more closely associated with what happens to the whole organism in an absence of RA signaling.

Data from the Angiogenesis Profiler Plate reported no significant difference in *Ctgf* expression (a P value of 0.498) in *Rdh10* conditional knockdowns relative to control, thus indicating that *Ctgf* is unchanged in the embryo of an *Rdh10* mutant. Therefore, *in vitro* analysis shows significant expression reduction in the absence of RA signaling while *in vivo* analysis does not. Perhaps when the organ has the surrounding tissue to support its development it is able to compensate for lack of RA signaling with some unknown mechanism. Pan-RAR inhibitors eliminate the possibility for RA signaling, while *Rdh10* conditional knockouts still allow alternative sources of RA to coactivate the RAR-RXR complex, such as carotenoids. Lack of change in an *Rdh10* mutant of *Ctgf* transcript abundance does not necessarily mean the protein product is not a target of RA signaling; instead, this phenomenon could indicate that CTGF is such a critical protein for salivary gland organogenesis that the organism has evolved compensatory mechanisms such as the use of alternative transcriptional activators or homologues to

adjust for reduced RA. Regardless, CTGF necessity for salivary gland development is currently being explored by the Sandell Lab.

Because the characterization of this study's principal candidate gene *Ctgf* revealed that there is no change in expression in *Rdh10* mutants relative to control, additional candidate gene expression analyses were conducted on the other genes identified to be targets of RA signaling in cultured assays. Of these genes, many are known to facilitate angiogenesis; those genes enabling angiogenesis were chosen as candidates for further investigation into how RA signaling gives rise to the vascular phenotype of *Rdh10* mutants. These genes were grouped into two categories: those involved in extracellular matrix processes and those involved in the production of developmental growth factors. The former group includes *Mmp2, Thb2,* and *Vtn.* Extracellular matrix proteins contribute to blood vessel construction, and many of these genes were hypothesized to experience reduction in transcript abundance in *Rdh10* knockouts. However, the expression rates of these genes remain unchanged in the mutants, and thus the vascular phenotype is not due to altered regulation of them.

Genes grouped by their involvement in the production of SMG developmental growth factors were similarly analyzed using qPCR to quantify their expression in mutant glands. These genes include *Bmp4, Igf1, Fgf8, Bmp2, Fgf7,* and *Fgfr2b.* The protein products of these genes have been shown to influence salivary gland epithelial morphogenesis during development (Lombaert, et al, 2010), while some such as Fibroblast Growth Factor Receptor 2, encoded by *Fgfr2b,* are involved in the formation of blood vessels (Santos-Ocampo, 1996). Although their functions varry, each gene fascilitates either the construction of blood vessel formation by primary action or by

enabling secondary mechanisms that give rise to vasculogenesis. Regardless, the expression rates of all genes within this category were not altered in *Rdh10* mutant qPCR analyses, and thus the vascular phenotype associated with *Rdh10* mutants is not due to altered regulation of these genes.

Because our qPCR experiments did not identify a gene target for RA signaling involved in angiogenesis, a qPCR array comparing expression of identified endothelial genes in *Rdh10* knockdowns compared to controls was performed to identify novel angiogenic genes mis-regulated in *Rdh10* mutant SMG. The purpose of this experiment was to identify genes that experience dysregulation in the absence of RA signaling and consequently give rise to aberrant vasculogenesis. Analysis of the profiler plate reported five genes with significant reductions of transcript abundance in mutant samples: *Angpt2, Jag1, Mapk14, Ptgs1,* and *S1pr1* (Fig. 11, 12). Additionally, the data from the profiler plate confirmed the findings of the previous qPCR analyses of genes involved in extracellular matrix processes and production of developmental growth factors.

Except for *S1pr1*, all genes experienced a decrease in transcript abundance in mutants. Oddly, the gene product of *Angpt2* functions as an antagonist of angiopoietin 1, which results in vascular remodeling disruption and in some cases endothelial cell apoptosis (Maisonpierre, et al, 1997), yet is downregulated in mutants. The gene product of *Jag1* is one of five ligands for receptors in the NOTCH signaling pathway which influences cellular fate during development (Lindsell, Shawber, Boulter, & Weinmaster, 1995), while the product of *Mapk14* is a stress-activated kinase involved in integration of biochemical signals for proliferation, differentiation, and trascription regulation (Kyriakis, Avruch, 2001). *Ptgs1* encodes cyclooxygenase, a critical enzyme in

prostaglandin biosynthesis (Wlodawer, Samuelsson, 1973). *S1pr1* encodes sphingozine-1-phosphate receptor 1 and aids in regulating endothelial cell cytoskeletal structure, migration, capillary-like network formation and vascular maturation (Lee, Thangada, Claffey, Ancellin, Liu, Kluk, Volpi, Sha'afi, & Hla, 1999).

To supplement experiments being conducted in the Sandell Lab, this study also searched for changes in expression upon conditional elimination of *Rdh10* of genes transcribing proteins involved in the metabolism of Vitamin A. Three genes were identified to experience significant changes in expression rates relative to control: *Aldh1a1, Aldh1a2,* and *Cyp26a1*. With the exception of *Aldh1a2*, loss of RA signaling resulted in reduced transcript abundance. RA is often eliminated by action of CYP26 family enzymes *(*Metzler & Sandell, 2016), and in the absence of RA the cell appears to downregulate the protein's production. Oxidation of all-*trans*-retinal (RAL) to RA, the third step in Vitamin A metabolism, is mediated by the ALDH1A family of enzymes, which includes *Aldh1a1, Aldh1a2,* and *Aldh1a3* (Metzler & Sandell, 2016). The ALDH1A1 enzyme is predominantly found in salivary gland epithelium, and thus its reduced transcript abundance in *Rdh10* knockdowns may contribute to the known epithelial branching defects observed in RA deficient mice. The ALDHIA2 enzyme is predominantly found in salivary gland mesenchyme where development in *Rdh10* knockdowns is not typically impaired, and thus its increased trasncript abundance in such mutants likely results from the organism compensating for loss of RDH10.

A total of 18 genes were tested during the scope of this study, and the data analysis of their Ct values can be found in the supplemental figures

CONCLUSION

Knowledge presented in this study regarding how RA signaling influences development of salivary gland vasculature will inform potential therapies for regeneration of damaged salivary glands. Further studies should characterize the angiogenic gene targets of RA signaling identified in this study in respect to the developing salivary gland, which include: *Angpt2, Jag1, Mapk14, Ptgs1, S1pr,* and *Fgfr2b.*

REFERENCES

Abashev, T. M., Metzler, M. A., Wright, D. M., & Sandell, L. L. (2017). Retinoic acid signaling regulates Krt5 and Krt14 independently of stem cell markers in submandibular salivary gland epithelium. *Dev Dyn, 246*(2), 135-147. doi:10.1002/dvdy.24476

Cady, J. (2007). Nutritional support during radiotherapy for head and neck cancer: the role of prophylactic feeding tube placement. *Clin J Oncol Nurs, 11*(6), 875-880. doi:10.1188/07.CJON.875-880

Delacroix L, Moutier E, Altobelli G, Legras S, Poch O, Choukralla MA, Bertin I, Jost B, Davidson I. (2009). Cell-Specific Interaction of Retinoic Acid Receptors with Target Genes in Mouse Embryonic Fibroblasts and Embyronic Stem Cells. *American Society for Microbiology Journals,* vol. 30 No. 1 231-244.

Hall-Glenn, Faith et al. (2012). CCN2/connective tissue growth factor is essential for pericyte adhesion and endothelial basement membrane formation during angiogenesis. *PloS one* vol. 7,2: e30562.

Hancock, P. J., Epstein, J. B., & Sadler, G. R. (2003). Oral and dental management related to radiation therapy for head and neck cancer. *J Can Dent Assoc, 69*(9), 585-590.

Holmberg, Kyle V and Matthew P Hoffman. (2014). "Anatomy, biogenesis and regeneration of salivary glands" *Monographs in oral science* vol. 24: 1-13. doi: 10.1159/000358776

Klein, E.S., Pino, M.E., Johnson, A. T., Davies, P.J.A., Nagpal, S., Thacher, S.M., Krasinski, G. and Chandraratna, R. A. S. (1996). Identification and functional

separation of retinoic acid receptor neutral antagonists and inverse agonists. *J. Biol. Chem.* 271, 22692-22696. doi:10.1074/jbc.271.37.22692

Kwon, H. R., Nelson, D. A., DeSantis, K. A., Morrissey, J. M., & Larsen, M. (2017). Endothelial cell regulation of salivary gland epithelial patterning. *Development, 144*(2), 211-220. doi:10.1242/dev.142497

Kyriakis JM, Avruch J. (2001). Mammalian mitogen-activated protein kinase signal transduction pathways activated by stress and inflammation. Physiological Reviews. 81 (2): 807–69. doi:10.1152/physrev.2001.81.2.807. PMID 11274345.

 Lee MJ, Thangada S, Claffey KP, Ancellin N, Liu CH, Kluk M, Volpi M, Sha'afi RI, Hla T. 1999. Vascular endothelial cell adherens junction assembly and morphogenesis induced by sphingosine-1-phosphate. Cell. 99 (3): 301–12. doi:10.1016/S0092-8674(00)81661-X. PMID 10555146.

Lindsell CE, Shawber CJ, Boulter J, Weinmaster G. 1995. Jagged: a mammalian ligand that activates Notch1. Cell. 80 (6): 909–17. doi:10.1016/0092-8674(95)90294-5. PMID 7697721.

Lombaert, Isabelle & P Hoffman, Matthew. (2010). Epithelial Stem/Progenitor Cells in the Embryonic Mouse Submandibular Gland. Frontiers of oral biology. 14. 90-106. 10.1159/000313709.

Lombaert, Isabelle et al. (2016). Concise Review: Salivary Gland Regeneration: Therapeutic Approaches from Stem Cells to Tissue Organoids. *Stem cells* (Dayton, Ohio) vol. 35,1 (2016): 97-105.

Maisonpierre PC, Suri C, Jones PF, Bartunkova S, Wiegand SJ, Radziejewski C, Compton D, McClain J, Aldrich TH, Papadopoulos N, Daly TJ, Davis S, Sato TN,

Yancopoulos GD. (1997). Angiopoietin-2, a natural antagonist for Tie2 that

    disrupts in vivo angiogenesis. Science. 277 (5322): 55–

    60. doi:10.1126/science.277.5322.55. PMID 9204896.

Metzler, M.A., Raja, S., Elliott, K.H., Friedl, R.M., Tran, N.Q.H., Brugmann, S.A.,

    Larsen, M., Sandell, L.L. 2018. RDH10-mediated retinol metabolism and

    RARalpha-mediated retinoic acid signaling are required for submandibular

    salivary gland initiation. Development 145.

Metzler, M. A., & Sandell, L. L. (2016). Enzymatic Metabolism of Vitamin A in

    Developing Vertebrate Embryos. *Nutrients, 8*(12). doi:10.3390/nu8120812

NIDCR, National Institute of Dental and Craniofacial Research. Salivary Gland

    Molecular Anatomy Project, Salivary Gland Gene Expression. Bethesda, MD

    20892-2190.

Nguyen, N. P., Vos, P., Karlsson, U., Nguyen, P., Dutta, S., Lemanski, C., . . . Sallah, S.

    (2007). Quality of life following chemoradiation and postoperative radiation for

    locally advanced head and neck cancer. *ORL J Otorhinolaryngol Relat Spec,*

    69(5), 271-276. doi:10.1159/000103870

Niederreither, K., & Dolle, P. (2008). Retinoic acid in development: towards an

    integrated view. *Nat Rev Genet, 9*(7), 541-553. doi:10.1038/nrg2340

Patel, R., & Shahane, A. (2014). The epidemiology of Sjogren's syndrome. *Clin*

    Epidemiol, 6, 247-255. doi:10.2147/CLEP.S47399

Ponticos, M. (2013). Connective tissue growth factor (CCN2) in blood vessels. *Vascul*

    Pharmacol, 58(3), 189-193. doi:10.1016/j.vph.2013.01.004

Sandell, L. L., Lynn, M. L., Inman, K. E., McDowell, W., & Trainor, P. A. (2012). RDH10 oxidation of Vitamin A is a critical control step in synthesis of retinoic acid during mouse embryogenesis. *PLoS One, 7*(2), e30698. doi:10.1371/journal.pone.0030698

Sandell, L. L., Sanderson, B. W., Moiseyev, G., Johnson, T., Mushegian, A., Young, K., . . . Trainor, P. A. (2007). RDH10 is essential for synthesis of embryonic retinoic acid and is required for limb, craniofacial, and organ development. *Genes Dev, 21*(9), 1113-1124. doi:10.1101/gad.1533407

Santos-Ocampo S, Colvin JS, Chellaiah A, Ornitz DM (1996). Expression and biological activity of mouse fibroblast growth factor-9. *The Journal of Biological Chemistry, 271 (3): 1726-31.* doi:10.1074/jbc.271.3.1726. PMID 8576175.

Seiwert, T. Y., Salama, J. K., & Vokes, E. E. (2007). The chemoradiation paradigm in head and neck cancer. *Nat Clin Pract Oncol, 4*(3), 156-171. doi:10.1038/ncponc0750

Tucker, A. S. (2007). Salivary gland development. *Semin Cell Dev Biol, 18*(2), 237-244. doi:10.1016/j.semcdb.2007.01.006

Ventura, A., Kirsch, D.G., McLaughlin, M.E., Tuveson, D.A., Grimm, J., Lintault, L., Newman, J., Reczek, E.E., Weissleder, R., Jacks, T., (2007). Restoration of p53 function leads to tumour regression in vivo. Nature 445, 661-665.

Wlodawer P, Samuelsson B. (1973). On the organization and mechanism of prostaglandin synthetase. *The Journal of Biological Chemistry. 248 (16): 5673–8. PMID 4723909.*

Wright, D. M., Buenger, D. E., Abashev, T. M., Lindeman, R. P., Ding, J., & Sandell, L.
L. (2015). Retinoic acid regulates embryonic development of mammalian
submandibular salivary glands. *Dev Biol, 407*(1), 57-67.
doi:10.1016/j.ydbio.2015.08.008

Wu S, Platteau A, Chen S, McNamara G, Whitsett J, Bancalari E. (2010). *Conditional
Overexpression of Connective Tissue Growth Fact Disrupts Postnatal Lung
Development. American Journal of Respiratory Cell and Molecular Biology. Vol.
42, 552-563.* doi.org/10.1165/rcmb.2009-0068OC

Sample	Mmp2	Gapdh	deltaCT	Average	deltadeltaC	2^(-deltade	Average	stdev	SEM
Het42	25.8604	20.63793	5.222467		0.838944	0.559052			
Het58	24.05577	19.8375	4.218267		-0.16526	1.121365			
Het95	24.57703	20.8672	3.709833	4.383522	-0.67369	1.595146	1.091855	0.518677	0.299458
Mut42	24.4606	20.6348	3.8258		-0.55772	1.471943			
Mut58	24.38587	19.56327	4.8226		0.439078	0.737606			
Mut95	24.37743	20.0133	4.364133		-0.01939	1.01353	1.07436	0.370929	0.262286

Supplement to Figure 9.

Sample	Thbs2	Gapdh	deltaCT	Average	deltadeltaC	2^(-deltade	Average	stdev	SEM
Het42	26.494	20.63793	5.856067		-0.35888	1.282433			
Het58	27.06455	19.8375	7.22705		1.0121	0.495824			
Het95	26.42893	20.8672	5.561733	6.21495	-0.65322	1.572671	1.116976	0.557164	0.321679
Mut42	26.48867	20.6348	5.853867		-0.36108	1.28439			
Mut58	25.8131	19.56327	6.249833		0.034883	0.976111			
Mut95	26.0604	20.0133	6.0471		-0.16785	1.123383	1.127961	0.154191	0.109029

Supplement to Figure 9.

Sample	Vtn	Gapdh	deltaCT	Average	deltadeltaC	2^(-deltade	Average	stdev	SEM
Het42	28.57265	20.04605	8.5266		0.298767	0.812947			
Het58	27.46713	19.13675	8.330383		0.10255	0.931385			
Het95	28.24317	20.41665	7.826517	8.227833	-0.40132	1.320713	1.021682	0.265653	0.153375
Mut42	28.59347	20.32835	8.265117		0.037283	0.974488			
Mut58	27.7303	19.56327	8.167033		-0.0608	1.043044			
Mut95	26.961	20.0133	6.9477		-1.28013	2.428614	1.482049	0.820466	0.580157

Supplement to Figure 9.

Samples	Bmp4	Gapdh Ct V	Delta CT	Control Ave	Delta Delta CT	2^-(deltadeltct)	Average	stdev	SEM
Het 42	27.9277	21.16627	6.761433		-0.4298	1.347046824			
Het 58	26.81907	19.48497	7.3341		0.142866667	0.905717685			
Het 95	27.85537	20.3772	7.478167	7.191233	0.286933333	0.819642482	1.024136	0.282942	0.591285
Mut 42	27.15063	20.63083	6.5198	6.977711	-0.671433333	1.592654501			
Mut 58	26.87933	19.5038	7.375533		0.1843	0.880075988			
Mut 95	26.6508	19.613	7.0378		-0.153433333	1.112213176	1.194981	0.363428	0.689923

Supplement to Figure 10.

Samples	Igf1	Gapdh Ct V	Delta CT	Control Ave	Delta Delta	2^-(deltade	Average	stdev	SEM
Het 42	24.4631	21.16627	3.296833		-0.28303	1.21675			
Het 58	23.5028	19.48497	4.017833		0.437967	0.738174			
Het 95	23.80213	20.3772	3.424933	3.579867	-0.15493	1.11337	1.022765	0.251825	0.590494
Mut 42	23.80963	20.63083	3.1788	3.454533	-0.40107	1.320484			
Mut 58	23.20157	19.5038	3.697767		0.1179	0.921528			
Mut 95	23.10003	19.613	3.487033		-0.09283	1.066463	1.102825	0.201948	0.636716

Supplement to Figure 10.

Samples	Fgf8	Gapdh Ct V	Delta CT	Control Ave	Delta Delta	2^-(deltade	Average	stdev	SEM
Het 42	33.3284	21.16627	12.16213		-1.42337	2.682107			
Het 58	33.61293	19.48497	14.12797		0.542467	0.686596			
Het 95	34.8436	20.3772	14.4664	13.5855	0.8809	0.543029	1.30391	1.19571	0.752813
Mut 42	32.38767	20.63083	11.75683	14.06239	-1.82867	3.552086			
Mut 58	35.09817	19.5038	15.59437		2.008867	0.248468			
Mut 95	34.44897	19.613	14.83597		1.250467	0.420312	1.406956	1.859724	0.812306

Supplement to Figure 10. Highlighted samples represent outliers referenced in Results

section under Figure 10.

Sample	Bmp2	CT Gapdh	deltaCT	Avg deltaCT Het	deltadelta	2^(-deltadeltaCT)	Average	stdev	SEM
Het 42	29.6241	20.73097	8.893133		-0.1798	1.132726845			
Het 58	28.64493	19.41947	9.225467		0.152533	0.89966928			
Het 95	29.30747	20.20727	9.1002	9.072933333	0.027267	0.981277668	1.004558	0.11826	0.068277
Mut 42	29.57503	20.86393	8.7111		-0.36183	1.285057873			
Mut 58	29.37843	19.76767	9.610767		0.537833	0.688804592			
Mut 95	28.6584	19.5254	9.133		0.060067	0.959219793	0.977694	0.298556	0.172371

Supplement to Figure 10.

Sample	Fgf7	CT Gapdh	deltaCT	Avg deltaCT	deltadelta	2^(-deltade	Average	stdev	SEM
Het 42	27.93657	20.73097	7.2056		0.267656	0.830668			
Het 58	26.43253	19.41947	7.013067		0.075122	0.949262			
Het 95	26.80243	20.20727	6.595167	6.937944	-0.34278	1.268196	1.016042	0.226279	0.130642
Mut 42	27.26763	20.86393	6.4037		-0.53424	1.448184			
Mut 58	26.42817	19.76767	6.6605		-0.27744	1.212046			
Mut 95	26.98397	19.5254	7.458567		0.520622	0.697071	1.1191	0.384085	0.221752

Supplement to Figure 10.

Sample	Fgfr2b	CT Gapdh	deltaCT	Avg deltaCT	deltadelta	2^(-deltade	Average	stdev	SEM
Het 42	26.39213	20.73097	5.661167		-0.3692	1.291636			
Het 58	25.72023	19.41947	6.300767		0.2704	0.82909			
Het 95	26.33643	20.20727	6.129167	6.030367	0.0988	0.933809	1.018178	0.242541	0.140031
Mut 42	27.3854	20.86393	6.521467		0.4911	0.711482			
Mut 58	25.96617	19.76767	6.1985		0.168133	0.889993			
Mut 95	26.5885	19.5254	7.0631		1.032733	0.488783	0.696753	0.20101	0.116053

Supplement to Figure 10.

sample	Aldh1a1	Gapdh	deltaCT	average	deltadeltaCT	2^(-deltadeltaCT)	Average	stdev	SEM
Het 42	28.98723	20.67987	8.307367		0.674166667	0.626694107			
Het 95	28.32067	21.2048	7.115867		-0.517333333	1.431307184			
Het 58	27.81097	20.3346	7.476367	7.6332	-0.156833333	1.11483742	1.057613	0.405347	0.234027
Mut 42	30.75967	20.68363	10.07603		2.442833333	0.18392209			
Mut 95	30.1823	20.17447	10.00783		2.374633333	0.192825354			
Mut 58	29.15733	20.571	8.586333	9.556733	0.953133333	0.516509456	0.297752	0.189502	0.109409

Supplement to Figure 13.

sample	Aldh1a2	Gapdh	deltaCT	average	deltadeltaCT	2^(-deltadeltaCT)	Average	stdev	SEM
Het 42	24.79417	20.67987	4.1143		0.565388889	0.675773232			
Het 95	24.4856	21.2048	3.2808		-0.268111111	1.204230123			
Het 58	23.58623	20.3346	3.251633	3.548911	-0.297277778	1.228823556	1.036276	0.312446	0.180391
Mut 42	23.6748	20.68363	2.991167		-0.557744444	1.471966099			
Mut 95	22.8522	20.17447	2.677733		-0.871177778	1.829155565			
Mut 58	23.40377	20.571	2.832767		-0.716144444	1.642785871	1.647969	0.178651	0.103144

Supplement to Figure 13.

sample	Aldh1a3	Gapdh	deltaCT	average	deltadeltaC	2^(-deltade	Average	stdev	SEM
Het 42	28.15847	20.67987	7.4786		0.340167	0.78995			
Het 95	28.30107	21.2048	7.096267		-0.04217	1.029659			
Het 58	27.17503	20.3346	6.840433	7.138433	-0.298	1.229439	1.016349	0.220047	0.127044
Mut 42	27.76307	20.68363	7.079433		-0.059	1.041743			
Mut 95	27.04573	20.17447	6.871267		-0.26717	1.203442			
Mut 58	27.21833	20.571	6.647333	6.866011	-0.4911	1.405516	1.216901	0.182259	0.105228

Supplement to Figure 13.

Sample	Cyp26a1	Gapdh	deltaCT	average	deltadeltaCT	2^(-deltadeltaCT)	Average	stdev	SEM
Het 42	29.4387	21.20327	8.235433		0.295666667	0.814695776			
Het 58	28.91903	20.68047	8.238567		0.2988	0.81292829			
Het 95	28.65933	21.31403	7.3453	7.939767	-0.594466667	1.5099143	1.045846	0.401896	0.232035
Mut 42	30.14207	21.3645	8.777567		0.8378	0.559496108			
Mut 58	30.1764	21.209	8.9674		1.027633333	0.490514152			
Mut 95	32.0311	20.609	11.4221		3.482333333	0.08947737	0.379829	0.253807	0.146535

Supplement to Figure 13.

Sample	Cyp26b1	Gapdh	deltaCT	average	deltadeltaC	2^(-deltadeltaCT)	average	stdev	SEM
Het 42	27.78403	21.20327	6.580767		0.357978	0.780257499			
Het 58	26.47547	20.68047	5.795		-0.42779	1.345170354			
Het 95	27.60663	21.31403	6.2926	6.222789	0.069811	0.952762733	1.026064	0.289502	0.167144
Mut 42	28.02393	21.3645	6.659433		0.436644	0.738851101			
Mut 58	27.4279	21.209	6.2189		-0.00389	1.002699209			
Mut 95	27.64497	20.609	7.035967		0.813178	0.569126879	0.770226	0.218482	0.126141

Supplement to Figure 13.

Sample	Dhrs3	Gapdh	deltaCT	average	deltadeltaC	2^(-deltade	average	stdev	SEM
Het 42	28.94647	21.20327	7.7432		1.015989	0.494489			
Het 58	27.19197	20.68047	6.5115		-0.21571	1.161276			
Het 95	27.24097	21.31403	5.926933	6.727211	-0.80028	1.741436	1.132401	0.623975	0.360252
Mut 42	28.7269	21.3645	7.3624		0.635189	0.643857			
Mut 58	27.54003	21.209	6.331033		-0.39618	1.316017			
Mut 95	27.84337	20.609	7.234367		0.507156	0.703608	0.887827	0.372025	0.214788

Supplement to Figure 13.

sample	RARb	gapdh	deltaCT	average	deltadeltaC	2^(-deltade	Average	stdev	SEM
Het 42	25.2227	20.39855	4.82415		0.8703	0.547033			
Het 95	24.51433	21.40297	3.111367		-0.84248	1.793134			
Het 58	24.2335	20.30747	3.926033	3.95385	-0.02782	1.019468	1.119878	0.629089	0.363205
Mut 42	24.46797	20.76727	3.7007		-0.25315	1.191806			
Mut 95	24.06757	20.49805	3.569517		-0.38433	1.305256			
Mut 58	24.42217	21.1346	3.287567		-0.66628	1.586979	1.361347	0.20347	0.117473

Supplement to Figure 13.

sample	stra6	gapdh	deltaCT	average	deltadeltaCT	2^(-deltadeltaCT)	Average	stdev	SEM
Het 42	24.59493	20.39855	4.196383		0.7414	0.598158614			
Het 95	24.45653	21.40297	3.053567		-0.401416667	1.320804249			
Het 58	23.42247	20.30747	3.115	3.454983	-0.339983333	1.265741971	1.061568	0.402268	0.232249
Mut 42	24.80363	20.76727	4.036367		0.581383333	0.668322646			
Mut 95	23.75133	20.49805	3.253283		-0.2017	1.150052722			
Mut 58	23.7241	21.1346	2.5895		-0.865483333	1.821949957	1.213442	0.57942	0.334528

Supplement to Figure 13.

DeltaDelta CT values						
	Ct.B1275.H1	Ct.B1275.H2	Ct.B1299.H1	Ct.B1275.M1	Ct.B1275.M2	Ct.B1299.M1
S1pr1	0.0249	-0.0295	0.0046	-0.4925	-0.5125	-0.6327
Angpt2	0.00796667	0.20416667	-0.21213333	1.217866667	0.968266667	0.997366667
Jag1	0.1432	-0.0124	-0.1308	0.4718	0.2892	0.4119
Ptgs1	0.3526	0.0077	-0.3603	0.6339	0.9218	0.7807
Mapk14	-0.0716	0.0794	-0.0078	0.1655	0.1115	0.2594
Fold Change (2^-deltadeltaCT)						
	Ct.B1275.H1	Ct.B1275.H2	Ct.B1299.H1	Ct.B1275.M1	Ct.B1275.M2	Ct.B1299.M1
S1pr1	0.98288872	1.02065833	0.9968166	1.406880703	1.426520026	1.550463969
Angpt2	0.99449315	0.86803994	1.15839986	0.429917974	0.511119782	0.500913477
Jag1	0.90550844	1.00863207	1.09490067	0.72106439	0.818355726	0.751632836
Ptgs1	0.78317141	0.99467698	1.28369281	0.644431982	0.527850029	0.582084296
Mapk14	1.0508815	0.94645118	1.00542119	0.891619454	0.92562517	0.835435295
STATS						
	Avg. Het	stdev Het	Avg. mut	stdev mut		
S1pr1	1.00012122	0.01910042	1.46128823	0.077850239		
Angpt2	1.00697765	0.145582	0.48065041	0.044230954		
Jag1	1.00301373	0.09482103	0.76368432	0.049752685		
Ptgs1	1.02051373	0.25125897	0.58478877	0.058338011		
Mapk14	1.00091796	0.0523606	0.88422664	0.045547159		

Supplement to Figure 11.
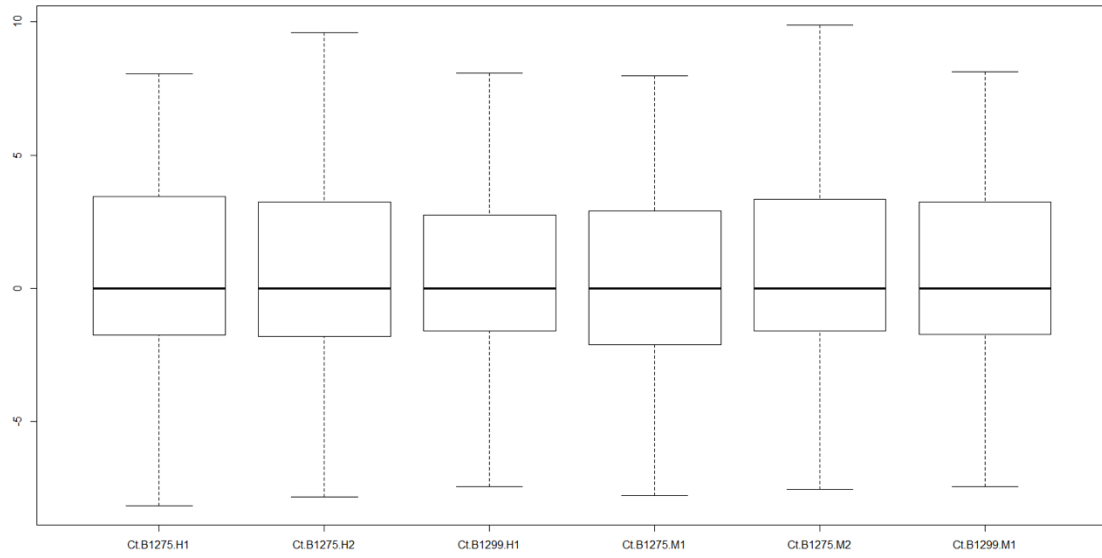
Supplement to Figure 12. Boxplots of sample medians normalized to Gapdh.

	Ct.B1275.H1	Ct.B1275.H2	Ct.B1299.H1	Ct.B1275.M1	Ct.B1275.M2	Ct.B1299.M1	p.value	t.statistic	log2 foldch
S1pr1	5.9914	5.937	5.9711	5.474	5.454	5.3338	0.000303	11.72205	0.5459
Angpt2	8.5574	8.7536	8.3373	9.7673	9.5177	9.5468	0.001796	-7.38145	-1.06117
Jag1	5.6459	5.4903	5.3719	5.9745	5.7919	5.9146	0.0151	-4.07991	-0.39097
Ptgs1	9.3267	8.9818	8.6138	9.608	9.8959	9.7548	0.024707	-3.50842	-0.7788
Mapk14	5.3609	5.5119	5.4247	5.598	5.544	5.6919	0.043798	-2.90727	-0.1788
Tnf	10.5096	10.8826	10.7022	12.0226	11.0812	11.3587	0.057755	-2.63711	-0.78937
Tgfa	10.6865	10.6077	9.5347	11.8848	11.0573	11.2672	0.065249	-2.52155	-1.1268
Nos3	8.0971	8.2776	8.2284	8.1366	7.937	7.9183	0.082085	2.309415	0.203733
Edn1	10.3318	9.7457	9.1095	10.7922	10.2616	11.1957	0.083332	-2.29571	-1.02083
Anpep	6.3818	6.3047	5.9777	6.9556	6.3321	6.8469	0.098777	-2.1428	-0.49013
F3	8.7465	8.9911	8.2054	9.0831	9.4659	9.0694	0.103738	-2.09928	-0.55847
Sphk1	8.4988	8.7148	7.6797	9.1381	8.7825	9.0174	0.109404	-2.0523	-0.68157
Pdgfa	3.812	4.0683	3.4761	4.1077	4.1224	4.6537	0.10964	-2.0504	-0.50913
B2m	4.298	4.0155	4.1422	4.0705	3.9092	3.7949	0.117955	1.986253	0.227033
Tgfb1	6.7671	6.655	6.1756	6.9016	6.9231	6.8377	0.12477	-1.93726	-0.3549
Igf1	3.3456	2.8091	2.5906	2.5145	2.5036	2.4407	0.129955	1.90189	0.428833
Tgfbf2	5.1353	4.4285	4.4652	4.3433	4.1547	4.2165	0.137356	1.853971	0.438167
Fgfr3	10.2621	10.8544	10.6917	10.7158	11.2173	11.1742	0.143816	-1.81436	-0.43303
Gusb	6.821	6.7937	6.2921	6.9493	6.8407	7.1755	0.149601	-1.78048	-0.3529
Fgf2	8.2062	7.7506	7.778	7.7848	7.5112	7.5493	0.157076	1.738701	0.2965
Mmp2	5.7267	5.7825	5.1058	6.0267	5.7793	5.9752	0.165674	-1.69318	-0.38873
Tgfb3	6.5014	6.3737	6.6157	6.5233	6.061	5.938	0.166926	1.686757	0.322833
Fgf1	12.0208	11.5408	10.9164	12.3586	11.636	12.5761	0.178259	-1.63084	-0.69757
Col18a1	4.5261	4.2651	4.0378	4.1337	4.0184	4.0327	0.214447	1.474171	0.214733
Cdh5	5.0916	4.6959	4.7658	4.7606	4.6571	4.564	0.22956	1.416568	0.190533
Serpine1	10.633	9.6736	10.3556	9.737	10.0376	9.5303	0.231315	1.410125	0.452433
Tbx1	8.9043	8.3223	8.2476	8.0833	8.4431	7.6519	0.234495	1.398577	0.431967
Vegfc	7.3721	6.8753	6.8531	7.2161	7.3384	7.2541	0.244704	-1.36252	-0.23603
Serpinf1	4.0474	3.8662	3.7366	3.8774	3.546	3.6986	0.251656	1.338807	0.176067
Flt1	7.7444	7.4852	7.7919	7.9605	7.6075	8.282	0.2718	-1.27354	-0.27617
Epas1	5.9621	5.8413	6.1246	5.9687	5.4935	5.8405	0.272546	1.271212	0.208433
Nrp1	5.1421	4.8934	4.5702	5.2367	5.0494	5.0023	0.275636	-1.26164	-0.22757
Hgf	9.217	9.5879	8.5687	9.584	9.4785	9.4267	0.284821	-1.23379	-0.37187
Plau	7.0625	6.5093	6.1708	7.2989	6.7738	6.806	0.289603	-1.21962	-0.3787
Tnfsf12	6.2326	5.7746	6.0184	6.0614	5.6951	5.7369	0.370014	1.009096	0.1774
Tek	7.6615	6.758	7.1337	7.2649	7.5826	7.5474	0.374067	-0.99961	-0.28057
Itgav	5.5047	5.3474	4.7217	5.4976	5.3376	5.4502	0.385675	-0.97294	-0.2372
Actb	-1.3148	-1.3427	-1.278	-1.0833	-1.4036	-1.1648	0.388691	-0.96613	-0.0946
Tgfbr1	5.7858	6.0946	5.7117	6.2295	6.0598	5.7896	0.402975	-0.93445	-0.16227
Kdr	5.128	4.6944	4.8174	4.7223	4.5585	4.9059	0.407743	0.924082	0.151033
Timp1	8.6077	8.6407	7.6873	8.1663	7.9691	7.9373	0.420229	0.897417	0.287667
Angpt1	12.6453	12.455	11.4123	12.0792	11.2372	11.9602	0.425526	0.886303	0.412
Pecam1	5.0579	4.5897	4.7276	4.8459	4.5447	4.563	0.454167	0.828089	0.140533
Efna1	6.8831	6.4955	6.4282	6.369	6.1637	6.7478	0.473923	0.789619	0.175433
Figf	11.6198	11.8952	10.8923	10.4633	11.8855	10.8793	0.489764	0.759664	0.393067
Ctgf	9.092	9.4602	8.4747	9.5254	8.9066	9.3572	0.498445	-0.74356	-0.2541
Pgf	9.92	9.0344	8.9143	9.0488	8.8375	9.2546	0.514014	0.715195	0.2426
Akt1	3.384	3.6721	2.9399	3.679	3.4289	3.3813	0.517867	-0.70827	-0.1644
Timp2	2.7926	2.5372	2.2902	2.6639	2.2221	2.3159	0.519786	0.704841	0.139367
Vegfb	4.5152	4.2644	3.8398	4.4006	4.3727	4.2686	0.522444	-0.7001	-0.14083
Mmp9	8.2408	8.1938	8.4353	8.3766	8.0787	8.9159	0.549413	-0.65295	-0.1671
Tie1	5.8284	5.4823	5.4649	5.9536	5.5245	5.6374	0.551889	-0.64871	-0.1133
Thbs1	5.0116	4.8398	4.6568	4.9787	4.8216	4.2292	0.55822	0.637911	0.159567
Ang	12.6401	11.7404	11.4751	12.2881	11.7207	12.6692	0.573227	-0.61265	-0.27413
Ptk2	5.1112	5.2695	4.8192	5.1263	5.2104	5.1073	0.580912	-0.59988	-0.08137
Vegfa	6.0856	5.7412	5.6357	5.6021	5.568	5.9799	0.611599	0.54998	0.104167
Smad5	5.0916	4.3669	4.0855	4.4633	4.2048	4.3793	0.620785	0.535351	0.165533
Hifla	4.2017	4.252	3.9982	4.3753	3.9557	4.3522	0.648548	-0.49192	-0.0771
Itgb3	7.1216	7.2808	6.6092	6.9138	6.7497	7.0301	0.652713	0.485504	0.106
Thbs2	6.8552	6.5147	6.6464	7.2816	6.8185	6.2929	0.699201	-0.41535	-0.12557
Mmp14	2.7217	2.4824	2.4854	2.8935	2.4017	2.5589	0.756568	-0.33198	-0.05487
Erbb2	5.8192	5.6107	5.3304	5.6359	5.5214	5.4546	0.759924	0.327199	0.049467
Ephb4	3.7282	3.5706	3.254	3.592	3.3429	3.4723	0.772503	0.309346	0.048533
Efnb2	2.6451	2.4614	1.8408	2.3425	1.9693	2.396	0.788163	0.287285	0.079833
Eng	5.4893	5.3689	5.1003	5.319	5.2947	5.4416	0.806999	-0.26097	-0.03227
Bai1	10.6838	10.3338	10.6957	10.8263	10.1997	10.8683	0.818791	-0.24461	-0.06033
Nrp2	2.4132	2.2796	1.9624	2.3626	2.0414	2.3761	0.821385	-0.24103	-0.04163
Lect1	9.8835	10.315	10.4565	10.2094	9.4898	10.7173	0.850537	0.200957	0.0795
Egf	11.56	12.2785	12.2349	11.979	12.223	12.0144	0.855055	-0.19478	-0.04767
Fn1	2.6517	2.2381	1.7721	2.1936	2.0037	2.3124	0.859848	0.188247	0.050733
Ccl2	12.44	11.8353	13.3544	12.1919	12.9054	12.8076	0.861945	-0.18539	-0.09173
Hsp90ab1	0.2427	0.1558	-0.326	0.2566	-0.0515	-0.0348	0.880316	-0.16043	-0.0326
Fgf6	14.8196	15.5993	10.7005	13.6626	14.645	13.4116	0.904549	-0.1277	-0.19993
Ccl11	6.3574	6.3099	5.9081	6.8873	5.7356	6.0812	0.913231	-0.11602	-0.0429
Cxcl5	12.9484	14.2246	12.8411	12.1015	13.7697	14.4168	0.916754	-0.11128	-0.0913
Mmp19	10.2143	11.3131	10.7995	10.5197	10.8557	11.0682	0.918095	-0.10948	-0.0389
Mdk	0.7837	0.7421	0.4843	0.792	0.5021	0.6935	0.955579	0.059271	0.0075
Gapdh	0	0	0	0	0	0	NA	NA	0

Supplement to Figure 12. Ct values, P values, t statistics, and log2 fold-change for genes examined in the Angiogenesis Profiler Plate. Highlighted P values indicate genes with statistically significant expression changes.

Primer Efficiencies

Primer	Efficiency	Slope
Bmp2	110.43%	-3.095
Bmp2 #2	101.05%	-3.2974
Bmp4	105.35%	-3.2
Fgf8	109.78%	-3.1079
Fgf2	84.35%	-3.7643
Fgf2 #2	106.90%	-3.1677
Igf1	101.44%	-3.2879

Primer Efficiency Figure 1. Assay efficiencies of the displayed primers were compared over a wide and narrow dynamic range of cDNA concentrations. Efficiencies were calculated using one-fifth dilution series. Initial primers for Bmp2 and Fgf2 displayed unacceptable efficiencies; alternative primers for those genes were then tested.
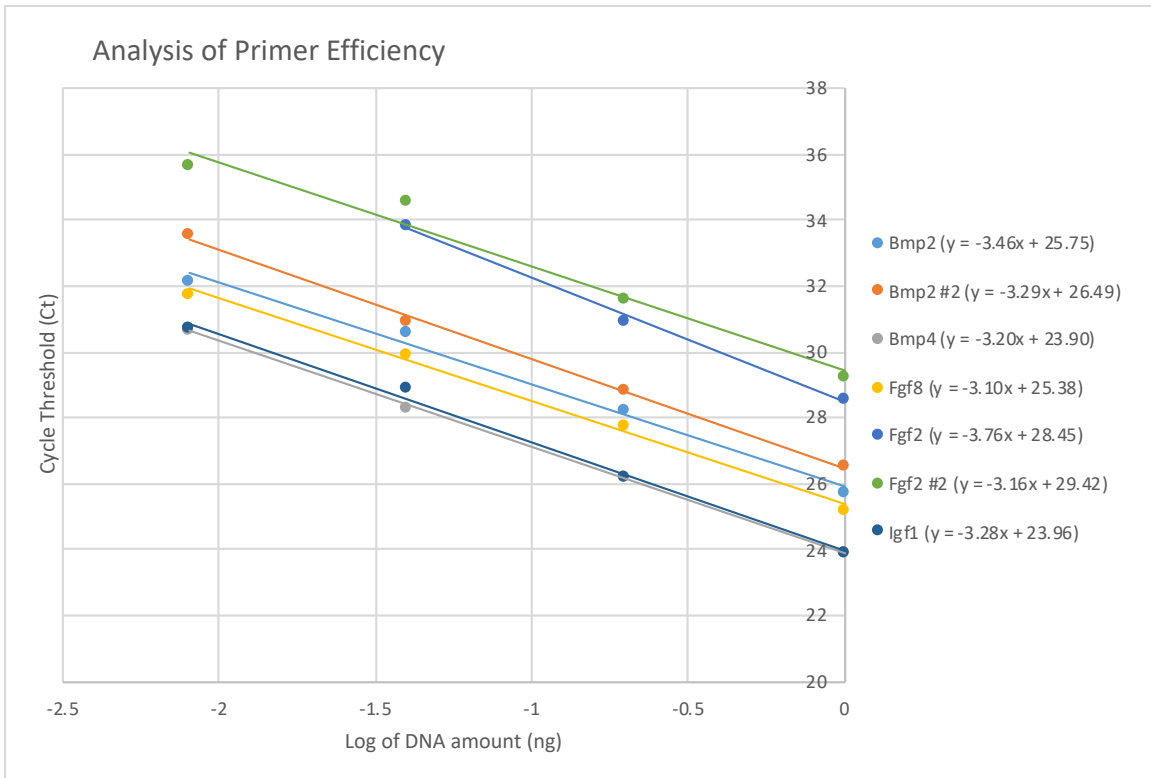
Primer Efficiency Figure 2. Analysis of primer efficiency.

Standard curves were generated by qPCR using a 5-fold serial dilution of heteroplasmic DNA (relative concentration of 1, .2, .04, .008 ng per reaction). First degree linear regressions were fitted for the log of input amount of template versus the Ct.